Tenascin-C increases lung metastasis by impacting blood vessel invasions

Zhen Sun, Inés Velázquez-Quesada, Devadarssen Murdamoothoo, Constance Ahowesso, Alev Yilmaz, Caroline Spenlé, Gerlinde Averous, William Erne, Felicitas Oberndorfer, Andre Oszwald, et al.

Version of Record: https://www.sciencedirect.com/science/article/pii/S0945053X19301283
Manuscript_f2173642bc7b0cb9a37b4d10b6e9f87b

Tenascin-C increases lung metastasis by impacting blood vessel invasions

Zhen Sun[1-4&*], Inés Velázquez-Quesada[1-4*], Devadarssen Murdamoothoo[1-4], Constance Ahowesso[1-4], Alev Yilmaz[1-4], Caroline Spenlé[1-4], Gerlinde Averous[5], William Erne[1-4], Felicitas Oberndorfer[6], Andre Oszwald[6], Renate Kain[6], Catherine Bourdon[7], Pierre Mangin[7], Claire Deligne[8], Kim Midwood[8], Chérine Abou-Faycal[1-4], Olivier Lefebvre[1-4], Annick Klein[1-4], Michael van der Heyden[1-4], Marie-Pierre Chenard[5], Gerhard Christofori[9], Carole Mathelin[10], Thomas Loustau[1-4], Thomas Hussenet[1-4] and Gertraud Orend[1-4#]

Running title: Through impacting blood vessel invasions tenascin-C increases metastasis

* equal contribution

correspondence:

Gertraud Orend, gertraud.orend@inserm.fr, Phone: +33 (0) 3 68 85 39 96, current address : Institut d'Hématologie et d'Immunologie, Hôpital Civil, 4 rue Kirschleger, 67085 Strasbourg Cedex

[&] Current address: 1. Tongji Cancer Research Institute, Tongji Hospital, Tongji Medical College in Huazhong University of Science and Technology, Wuhan, Hubei, China. 2. Department of Gastrointestinal Surgery, Tongji Hospital, Tongji Medical College in Huazhong University of Science and Technology, Wuhan, Hubei, China.

[1] INSERM U1109 - MN3T, The Microenvironmental Niche in Tumorigenesis and Targeted Therapy and, the Tumor Microenvironment group

[2] Université de Strasbourg, Strasbourg, France

[3] LabEx Medalis, Université de Strasbourg, France

[4] Fédération de Médecine Translationnelle de Strasbourg (FMTS), Strasbourg, France

[5] Department of Pathology, University Hospital Strasbourg, Strasbourg, France

[6] Department of Pathology, Medical University of Vienna (MUW), Vienna, Austria

[7] Etablissement Français du Sang, INSERM U949, Strasbourg, France

[8] Kennedy Institute of Rheumatology, University of Oxford, Oxford, UK

[9] Department Medicine, University Basel, Basel, Switzerland

[10] Department of breast diseases and surgery, Strasbourg University Hospital, Strasbourg, France

Keywords: Blood vessel invasions, circulating tumor cells, tumor emboli, tenascin-C, cellular plasticity, TGF-β signaling, lung metastasis, endothelialization, Fsp1+ cells, endothelial cells

Abbreviations:

BVI, blood vessel invasions

CD31, cluster of differentiation 31

CD41, cluster of differentiation 41, integrin alpha chain 2b

Cl. Cas-3, cleaved caspase-3

CK8/18, cytokeratin 8/18

DAPI, 4′,6-diamidino-2-phenylindole,

DMEM, Dulbecco's Modified Eagle's Medium

ELISA, Enzyme-linked immunosorbent assay

EPC, endothelial progenitor cells

EMT, epithelial-to-mesenchymal transition

ERK, extracellular signal-regulated kinases,

ECM, extracellular matrix

FN, fibronectin

Fsp1, fibroblast-specific protein 1

GAPDH, Glyceraldehyde 3-phosphate dehydrogenase

GW788388,

4-(4-[3-(Pyridin-2-yl)-1H-pyrazol-4-yl]pyridin-2-yl)-N-(tetrahydro-2Hpyran-4-yl) benzamide

HCC, hepatocellular carcinoma

HE, Hematoxylin and eosin

IDC NST, invasive ductal carcinoma, no special type

KD, knock down

KO, knock out

LM, laminin

LVI, lymph vessel invasions

MaCa, mammary carcinomas

Mmp9, Matrix metallopeptidase 9

MMTV-NeuNT, mouse mammary tumor virus driven NeuNT (activated rat ErbB2 homologue) transformed

NOS, not otherwise specified

NT193, MMTV-NeuNT breast tumor derived cell line

Pai-1, plasminogen activator inhibitor-1

PBS, phosphate-buffered saline

PDAC, pancreatic ductal adenocarcinomas

PNET, pancreatic neuroendocrine tumors

PyMT, polyoma middle T antigen

RAM1, reduced Arbuscular Mycorrhization 1

RCC, renal cell carcinoma

Sh, short hairpin

Slug, snail family zinc finger 2

Snail, snail family zinc finger 1

STS, staurosporine

TGF-β, transforming growth factor β

TME, tumor microenvironment

TNBC, triple negative breast cancer

TNC, tenascin-C

VEGFA, vascular endothelial growth factor A

WT, wild type

Zeb1, zinc finger E-box-binding homeobox 1

α-SMA, alpha-smooth muscle actin

Abstract

Metastasis is a major cause of death in cancer patients. The extracellular matrix molecule tenascin-C is a known promoter of metastasis, however the underlying mechanisms are not well understood. To further analyze the impact of tenascin-C on cancer progression we generated MMTV-NeuNT mice that develop spontaneous mammary tumors, on a tenascin-C knockout background. We also developed a syngeneic orthotopic model in which tumor cells derived from a MMTV-NeuNT tumor. Tumor cells were transfected with control shRNA or with shRNA to knockdown tenascin-C expression and, were grafted into the mammary gland of immune competent, wildtype or tenascin-C knockout mice. We show that stromal-derived TNC increases metastasis by reducing apoptosis and inducing the cellular plasticity of cancer cells located in pulmonary blood vessels invasions (BVI), before extravasation. We characterized BVI as organized structures of tightly packed aggregates of proliferating tumor cells with epithelial characteristics, surrounded by Fsp1+ cells, internally located platelets and, a luminal monolayer of endothelial cells. We found extracellular matrix, in particular, tenascin-C, between the stromal cells and the tumor cell cluster. In mice lacking stromal-derived tenascin-C, the organization of pulmonary BVI was significantly affected, revealing novel functions of host-derived tenascin-C in supporting the integrity of the endothelial cell coat, increasing platelet abundance, tumor cell survival, epithelial plasticity, thereby promoting overall lung metastasis. Many effects of tenascin-C observed in BVI including enhancement of cellular plasticity, survival and migration, could be explained by activation of TGF-β signaling. Finally, in several human cancers, we also observed BVI to be surrounded by an endothelial monolayer and to express tenascin-C. Expression of tenascin-C is specific to BVI and is not observed in lymphatic vascular invasions frequent in breast cancer, which lack an endothelial lining. Given that BVI have prognostic significance for many tumor types, such

as shorter cancer patient survival, increased metastasis, vessel occlusion, and organ failure, our data revealing a novel mechanism by which stromal tenascin-C promotes metastasis in human cancer, may have potential for diagnosis and therapy.

Introduction

Despite earlier diagnosis and improved treatment a high number of cancer patients die due to cancer-related complications, tumor recurrence and, most frequently, metastasis [1]. To improve patient survival a better knowledge of the mechanisms of metastasis is required. During metastasis, tumor cells disseminate from the primary tumor and invade blood or lymphatic vessels where they can be found as circulating tumor cells appearing in a variety of forms as ranging from single cells or small cell clusters up to multicellular tumor cell aggregates or tumor emboli. Tumor emboli can be classified as blood vessel invasions (BVI) or lymphatic vessel invasions (LVI), all together covered by the term lympho-vascular invasions [2–4]. The presence of vascular invasions in the primary tumor and the distant organ correlates with poorer cancer patient survival, increased metastasis, vessel occlusion and organ failure [5,6]. Therefore, targeting vascular invasions may offer novel treatment opportunities. To date, very little is known about the cellular composition of vascular invasions, nor whether there are differences in BVI in comparison to LVI.

The tumor microenvironment (TME) comprises tumor and stromal cells, soluble factors and extracellular matrix (ECM) [7]. An important ECM molecule that enhances metastasis is tenascin-C (TNC) [8,9]. As reviewed [10], TNC plays multiple roles in cancer. Recently, this has been comprehensively demonstrated in the first stochastic neuroendocrine tumor (PNET) model with abundant and no TNC, where TNC was found to enhance survival, proliferation, invasion, angiogenesis and lung metastasis [11].

By using breast cancer xenograft models, TNC was identified as a gene that mediates metastasis to the lung relevant during early steps of lung metastasis colonization; however, its relevance in immune competent breast cancer models with spontaneous

tumor onset has not been confirmed [8,9,12–14]. Moreover no model existed to address the relative contribution of host and tumor cell-derived TNC on breast cancer progression in an immune competent setting.

We have chosen the MMTV-NeuNT transgenic mouse model of metastatic cancer, ectopically expressing an active ErbB2 molecule from rat under control of the MMTV enhancer, that spontaneously develops primary mammary tumors and pulmonary BVI as precursors of parenchymal metastasis [15–17]. By using our novel cancer progression models, we observed that TNC increases lung metastasis by impacting BVI at multiple levels. In patients, we observed BVI in human cancers to be similarly organized to those in the mouse models, and also express TNC. Our results may offer novel opportunities for cancer diagnosis and therapy.

Results

1. 1 Tenascin-C accelerates tumor onset

We generated compound MMTV-NeuNT tumor mice deficient in *Tnc* (NeuNT-TNCKO) and compared tumorigenesis in these mice with mice expressing normal (wildtype, WT) levels of TNC (NeuNT-WT). By immunofluorescence staining of primary tumors we found TNC expressed in tumor matrix tracks (**Fig. S1A**) as previously shown in other cancers [18]. No TNC protein was found in TNCKO tumors (**Fig. S1A, B**). We compared tumor onset and observed that tumor latency was largely delayed in NeuNT-TNCKO mice (**Fig. 1A**). As previously described in this model all mice developed multiple tumors [16], the number of which was not affected by TNC. Mice were sacrificed 3 months after first tumor palpation and no significant difference in tumor burden, proliferation nor apoptosis between genotypes was noted (**Fig. 1B**, data not shown).

1.2 Tenascin-C enhances lung metastasis

We assessed lung metastasis by a stereological analysis [19] of the left and biggest lung lobe and observed no difference in the number of metastasis between NeuNT-TNCKO and NeuNT-WT mice (**Fig. 1C, D**). Yet, we found a larger lung surface covered by tumor cells in NeuNT-WT compared to NeuNT-TNCKO mice (**Fig. 1C, E**). As pulmonary BVI have been observed in Neu models [15] and were described as precursors of lung metastasis [17], we used immunohistochemistry to assess whether BVI are also common in the NeuNT model [16]. Indeed, we observed BVI in the lungs of these mice and, also in the primary tumors which had not been documented beforehand in any MMTV-Neu model (**Fig. 1C, F, Fig. S1C**). Surface measurement revealed that BVI are bigger in the lungs from NeuNT-WT mice than in those from NeuNT-TNCKO mice (**Fig. 1F, G**). As reduced proliferation and/or increased apoptosis could account for a difference in BVI

size, we performed staining for cleaved caspase-3 (Cl. Cas-3) and Ki67, respectively. We noticed that Cl. Cas-3+ cells are less abundant in BVI from NeuNT-WT than NeuNT-TNCKO mice, indicating that TNC promotes tumor cell survival in the BVI (**Fig. 1H, I**). It is remarkable that some tumor cells within the BVI proliferate, yet there is no difference in the number of Ki67+ cells between tumor mice expressing or lacking TNC (**Fig. 1J, K**). Similar to tumor cells in the BVI, also in the parenchymal metastasis TNC did not impact cell proliferation, but enhanced tumor cell survival (**Fig. S1D-G**). In summary, our data indicate that in the MMTV-NeuNT model TNC promotes cancer cell survival in pulmonary BVI as well as in parenchymal metastasis which could explain the observed larger metastatic surface in lungs from WT tumor mice.

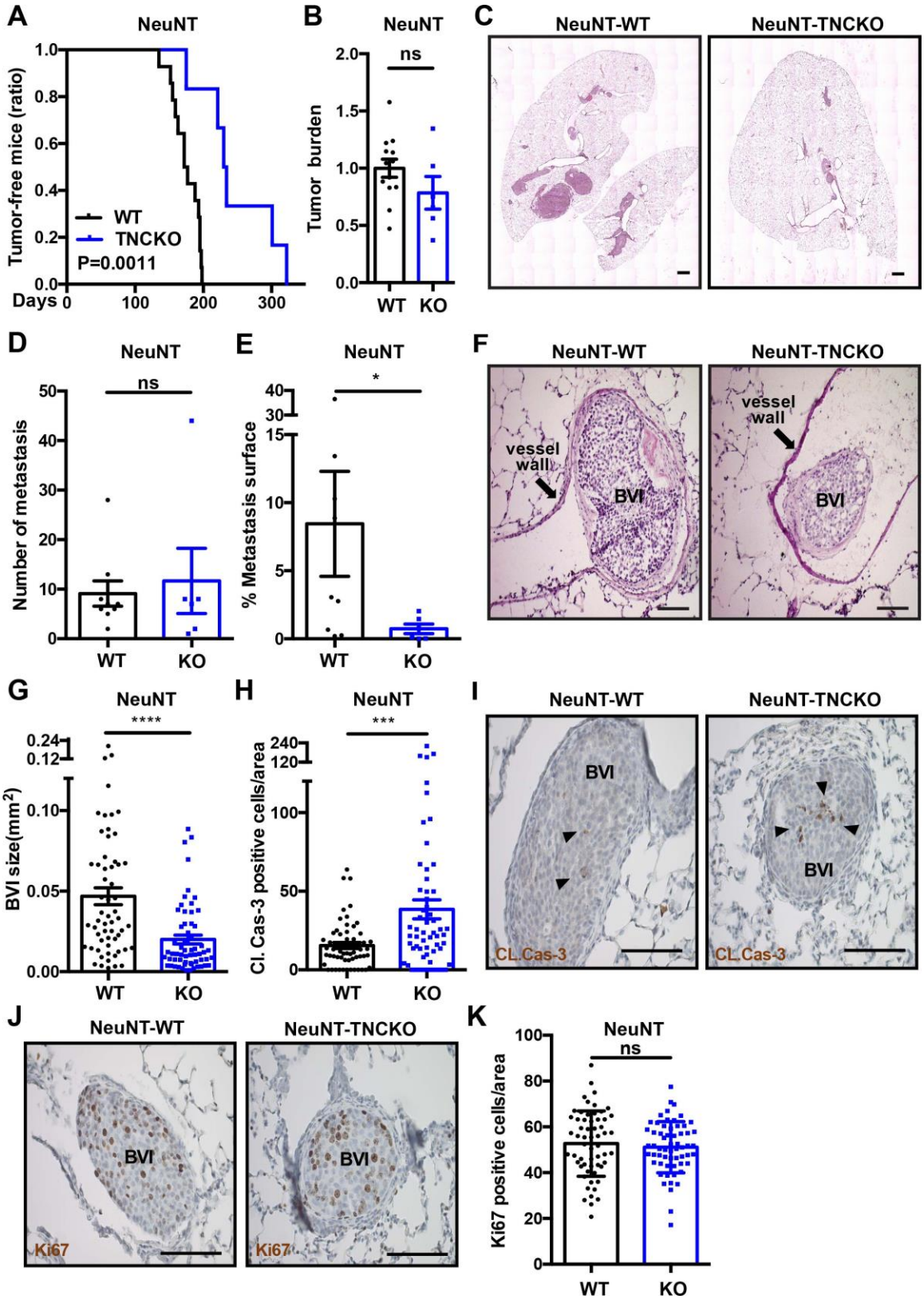
A
NeuNT
Tumor-free mice (ratio)
1.0
0.8
0.6
0.4
0.2
0.0
WT
TNCKO
P=0.0011
Days 0
100
200
300
B
NeuNT
ns
Tumor burden
2.0
1.5
1.0
0.5
0.0
WT
KO
C
NeuNT-WT
NeuNT-TNCKO
D
NeuNT
ns
Number of metastasis
50
40
30
20
10
0
WT
KO
E
NeuNT
*
% Metastasis surface
40
30
15
10
5
0
WT
KO
F
NeuNT-WT
NeuNT-TNCKO
vessel wall
BVI
vessel wall
BVI
G
NeuNT
****
BVI size(mm2)
0.24
0.12
0.10
0.05
0.00
WT
KO
H
NeuNT
***
Cl. Cas-3 positive cells/area
240
120
100
50
0
WT
KO
I
NeuNT-WT
NeuNT-TNCKO
BVI
BVI
CL.Cas-3
CL.Cas-3
J
NeuNT-WT
NeuNT-TNCKO
BVI
BVI
Ki67
Ki67
K
NeuNT
ns
Ki67 positive cells/area
100
80
60
40
20
0
WT
KO

Figure 1. Increased lung metastasis in the presence of TNC in MMTV-NeuNT mice

(A) Ratio of tumor-free mice is shown for MMTV-NeuNT tumor mice with two (NeuNT-WT, N = 13 mice) and no (NeuNT-TNCKO, N = 6) TNC alleles. The absence of TNC significantly delays tumor latency (NeuNT-WT versus NeuNT-TNCKO, p = 0.0011; Log-rank tests). **(B)** Tumor burden of NeuNT-TNCKO tumor mice (N = 6) was determined and normalized to the mean tumor weight of the control group (NeuNT-WT, N = 13). **(C)** Representative HE images of lung metastasis from MMTV-NeuNT mice (NeuNT-WT and NeuNT-TNCKO) that had been sacrificed 3 months after tumor detection. Scale bar: 1000 µm. **(D, E)** Number of lung metastases **(D)** and of the cumulated metastatic burden (metastatic area normalized to total lung area) **(E)** in lungs of NeuNT-WT (N = 9) and NeuNT-TNCKO (N = 6) mice. **(F, G)** HE stained lung tissue was used for BVI size determination (NeuNT-WT, N = 6 mice, n = 59 BVI; NeuNT-TNCKO, N = 6 mice, n = 60 BVI). Scale bar: 100 µm. **(H-K)** measurement of apoptosis and proliferation by IHC analysis for cleaved caspase-3 (Cl. Cas-3) **(H, I)** and Ki67 **(J, K)** in BVI (NeuNT-WT, N = 6 mice, n = 59 BVI; NeuNT-TNCKO, N = 6 mice, n = 60 BVI). Dots represent number of apoptotic **(H)** and proliferative cells **(K)** in BVI per area (0.1 mm^2), respectively. Arrowhead denotes Cl. Cas-3 positive apoptotic cell **(I)**. Scale bar, 100 µm. Mean ± SEM. **(B, D, E, G, H and K)** unpaired Student t or Mann-Whitney test.

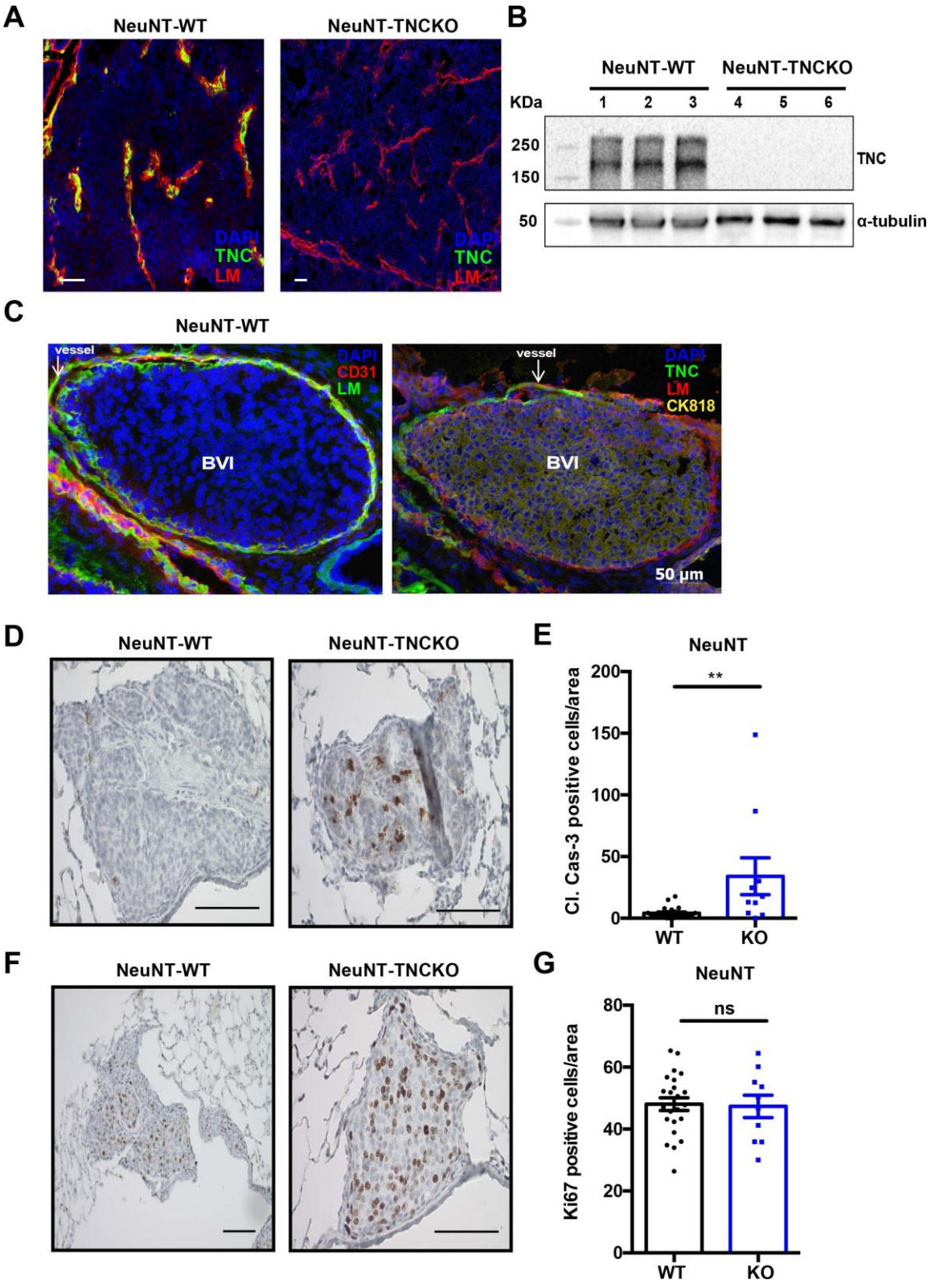

Figure S1. TNC promotes survival of cancer cells in parenchymal metastasis, yet not proliferation **(A)** Representative IF images for TNC (green) and laminin (red) of

primary tumors of MMTV-NeuNT mice (NeuNT-WT and NeuNT-TNCKO), respectively. Note, organisation of TNC into matrix tracks**. (B)** Representative immunoblot of TNC in MMTV-NeuNT breast tumors with α-tubulin as loading control. Note, no detection of TNC in NeuNT-TNCKO tumors. **(C)** Representative IF images of BVI in NeuNT-WT primary tumor stained for the indicated molecules. Note, two layers of LM, one from the blood vessel and another from the BVI that is occluding the vessel. (**D-G)** IHC analysis for cleaved caspase-3 (Cl. Cas-3) **(D)** and Ki67 **(F)** in lung parenchymal metastases (NeuNT-WT, N = 6 mice, n = 23 metastases; NeuNT-TNCKO, N = 6 mice, n = 10 metastases). A dot represents the accumulated number of apoptotic **(E)** and proliferative cells **(G)** per area (0.1 mm^2) in parenchymal metastasis. Scale bar, 100 μm. Mean ± SEM. Mann-Whitney test.

2. Host-derived tenascin-C promotes growth of BVI and overall metastasis

Previous reports using a xenograft model suggested that, host-derived TNC has a minor impact on lung metastasis colonization [8,9,14]. As tumor immunity largely impacts tumor growth and metastasis, which is missing in the xenograft models, we addressed how host- versus tumor cell-derived TNC impacts cancer progression in an immune competent setting. Therefore, we established a syngeneic orthotopic grafting model by using NT193 cells that we previously had established from a MMTV-NeuNT tumor [20].

We engineered NT193 cells to downregulate *Tnc* by shRNA technology. To mitigate possible off target effects we used two different shRNA sequences (sh1TNC and sh2TNC) and, grafted the tumor cells into the mammary gland of naïve WT and TNCKO FVB mice, respectively. We confirmed *Tnc* knockdown in the cultured cells by immunoblotting (**Fig. S2E**). Upon immunofluorescence analysis of the arising tumors in

the mammary gland we noticed that TNC levels are highest in a WT host upon engraftment of shC cells (transfected with a control shRNA sequence (shC), WT/shC or TNC-high tumors) and almost absent in KO/shTNC (or TNC-low) tumors, suggesting that the *Tnc* knockdown is stable *in vivo* (**Fig. S2F, G**). We further observed that mice with NT193 tumors develop spontaneously metastasis in the lung parenchyma as well as BVI in blood vessels of the lung. As for the MMTV-NeuNT model, with the changing levels of TNC expression we found no difference either in tumor burden (**Fig. S2H**) nor in lung metastasis incidence (**Fig. 2A**). Yet, we noticed that the lung metastasis surface is larger in TNC-high (WT/shC) than TNC-low (KO/shC) conditions. Moreover, irrespective of the cell genotype, there is a tendency towards more metastasis in WT than in TNCKO mice suggesting an involvement of host-derived TNC in promoting metastasis (**Fig. 2B**). Next, we determined the surface of the BVI and found that BVI derived from TNC-high (WT/shC) tumor mice are significantly bigger than from TNC-low (KO/shC) tumor mice (**Fig. 2C**). To address whether a difference in proliferation or survival accounts for the observed result we again stained for Ki67 and Cl. casp-3, respectively. As for the genetic MMTV-NeuNT model, in the BVI some tumor cells proliferate, yet independent of TNC (**Fig. 2D, E**). In contrast to proliferation, we saw that apoptosis is higher in BVI from KO tumor mice and, that in TNC-high (WT/shC) conditions apoptosis is the least (**Fig. 2F, G**). Altogether, these results demonstrate an important role of host-derived TNC in increasing BVI tumor cell survival and metastasis and, distinct functions of stromal and tumor cell derived TNC in metastasis.

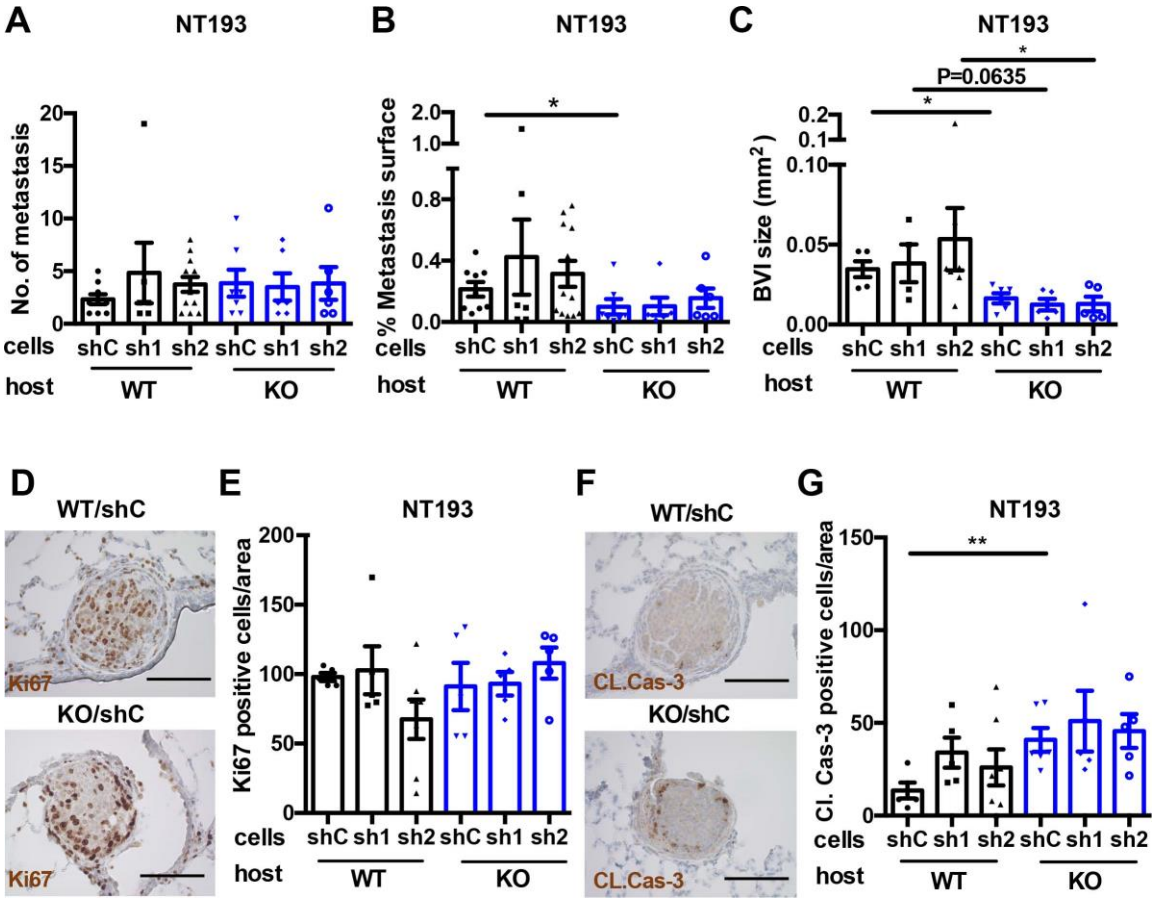

Figure 2. Host-derived TNC promotes lung metastasis in NT193 grafted tumor mice

(A-C) Quantification of the number of lung metastases (N, at least 5) **(A)**, cumulated metastatic burden (metastatic area normalized to total lung area) (N, at least 5) **(B)** and size of BVI **(C)** in lungs of WT and TNCKO FVB hosts after engraftment of NT193 sh control (shC), sh1TNC and sh2TNC cells (WT/shC (N = 5 mice); WT/sh1TNC (N = 4 mice); WT/sh2TNC (N = 7 mice); KO/shC (N = 6 mice); KO/sh1TNC (N = 5 mice); KO/sh2TNC (N = 5 mice). Note a bigger metastatic surface and bigger BVI in a WT host. **(D-G)** IHC analysis for Ki-67 **(D)** and cleaved caspase-3 (Cl. Cas-3) **(F)** in BVI of lungs from NT193 engrafted mice. Dots represent proliferative **(E)** and apoptotic cells in BVI **(G)** per 0.1 mm^2, respectively. Note more apoptotic cells in tumors of the KO host. Scale bar, 100 µm. Mean ± SEM, unpaired Student t or Mann-Whitney test. Statistical analysis was

performed between all groups. Only statistically significant ($p < 0.05$) differences are marked.

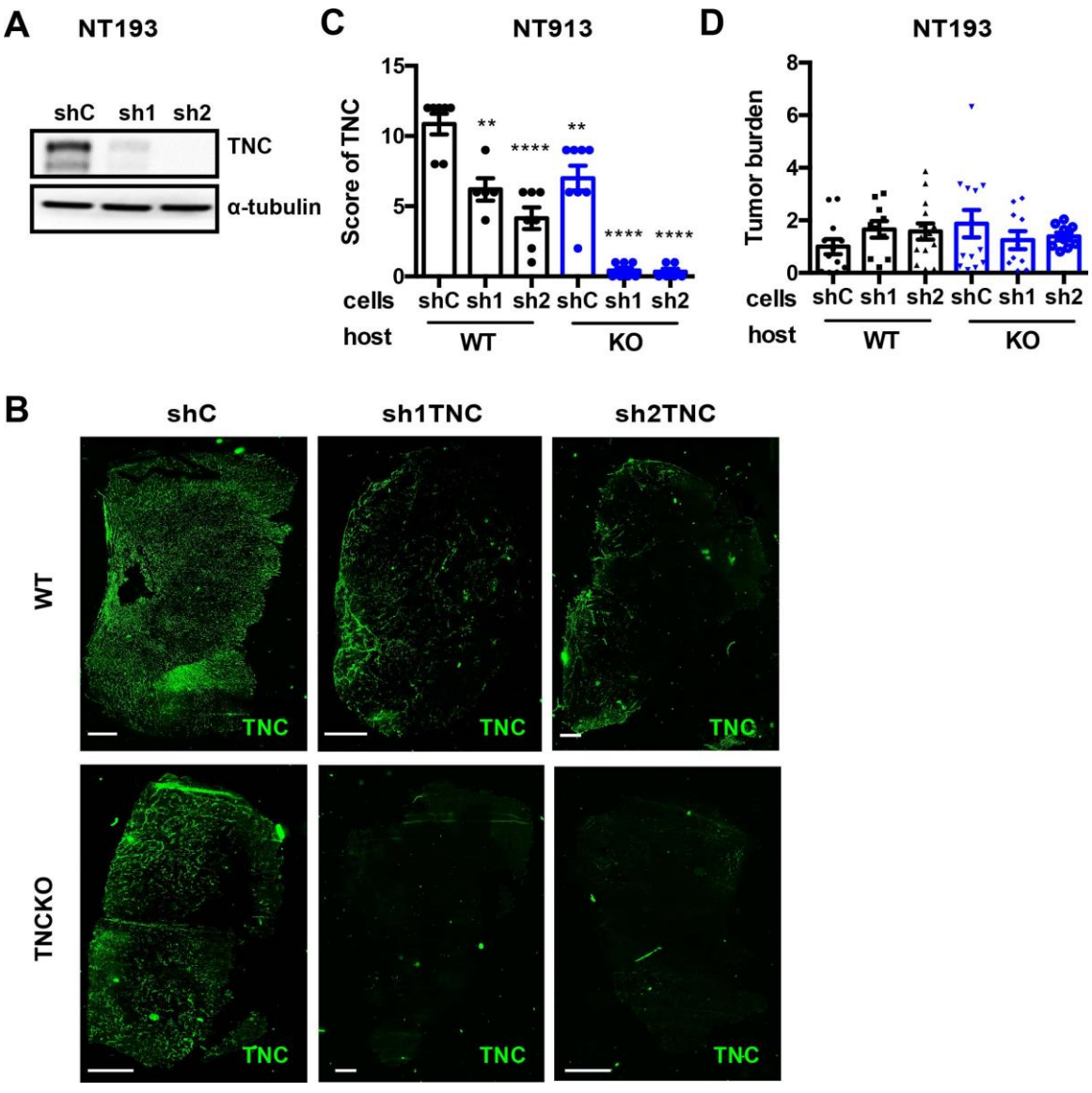

Figure S2. Stable knockdown of TNC in NT193 cells *in vitro* and in tumor grafts (A) Immunoblotting for TNC in cultured NT193 control (shC) and TNC knockdown cells (sh1 and sh2). Loading control, α–tubulin. **(B)** Representative mosaic IF images of TNC (green) in breast primary tumors, upon engraftment of NT193 shC and TNC knockdown

cells in the mammary fat pad of WT and TNCKO FVB mice, respectively. Scale bar, 1 mm. **(C)** TNC score in the primary tumor of each grafting condition (see material and methods for details). N, at least 6 mice for each grafting condition. Note a robust knockdown of TNC in vitro and in the tumors. **(D)** Relative tumor burden of TNCWT and TNCKO FVB mice upon engraftment of NT193 cells, WT/shC (N = 12); WT/sh1TNC (N = 10); WT/sh2TNC (N = 14); KO/shC (N = 13); KO/sh1TNC (N = 10); KO/sh2TNC (N = 9). Mean ± SEM, unpaired Student t or Mann-Whitney test. Statistical analysis was performed between all groups. Only statistically significant ($p < 0.05$) differences are marked, in comparison to WT/shC (**C**).

3. Tenascin-C surrounds epithelial tumor cell aggregates in BVI

To understand the composition of pulmonary BVI, we analyzed tumor and lung tissue of NeuNT-WT mice. BVI were found in blood vessels of the primary tumor (**Fig. S1C**), and the lung, sometimes surrounded by a thick ECM layer (**Fig. 3A**). BVI also could completely occlude the vessel lumen and had an eventual necrotic center (**Fig. 3A, S3A-C, Fig. S1C**).

The core of the BVI is composed of cancer cells (ErbB2+) with epithelial phenotype (CK8/18+) (**Fig. 3B - D**). We addressed by staining whether BVI express TNC and saw indeed abundant TNC at the periphery, yet no TNC within the tumor cell cluster that homogenously expresses ErbB2 (**Fig. 3B - D**). We also noticed the absence of TNC when tumor cells are extravasating from the BVI into the lung parenchyma (**Fig. 3B**).

Since we observed that host-derived TNC promotes BVI growth we wondered which stromal cells could be a source of TNC. Considering that Fsp1+ fibroblasts/myeloid cells were described in another breast cancer model as a source of TNC (and other molecules such as VEGFA) and, have been shown to promote tumor progression [21], we

evaluated their presence in BVI. Indeed, we observed Fsp1+ cells in BVI and, an overlap of the signals for Fsp1 and TNC, suggesting that Fsp1+ cells are a likely source of TNC in BVI (**Fig. 3D**). A similar result was obtained in the NT193 grafting model, where the Fsp1 signal also co-localized with TNC (**Fig. 3E**). Of note, Fsp1+ cells are also present in BVI from NeuNT mice deficient in TNC (**Fig. S3E**).

Together, Fsp1-expressing cells are likely candidates to express TNC in BVI of both models. This result also demonstrates a strong similarity between the genetic and grafting model.

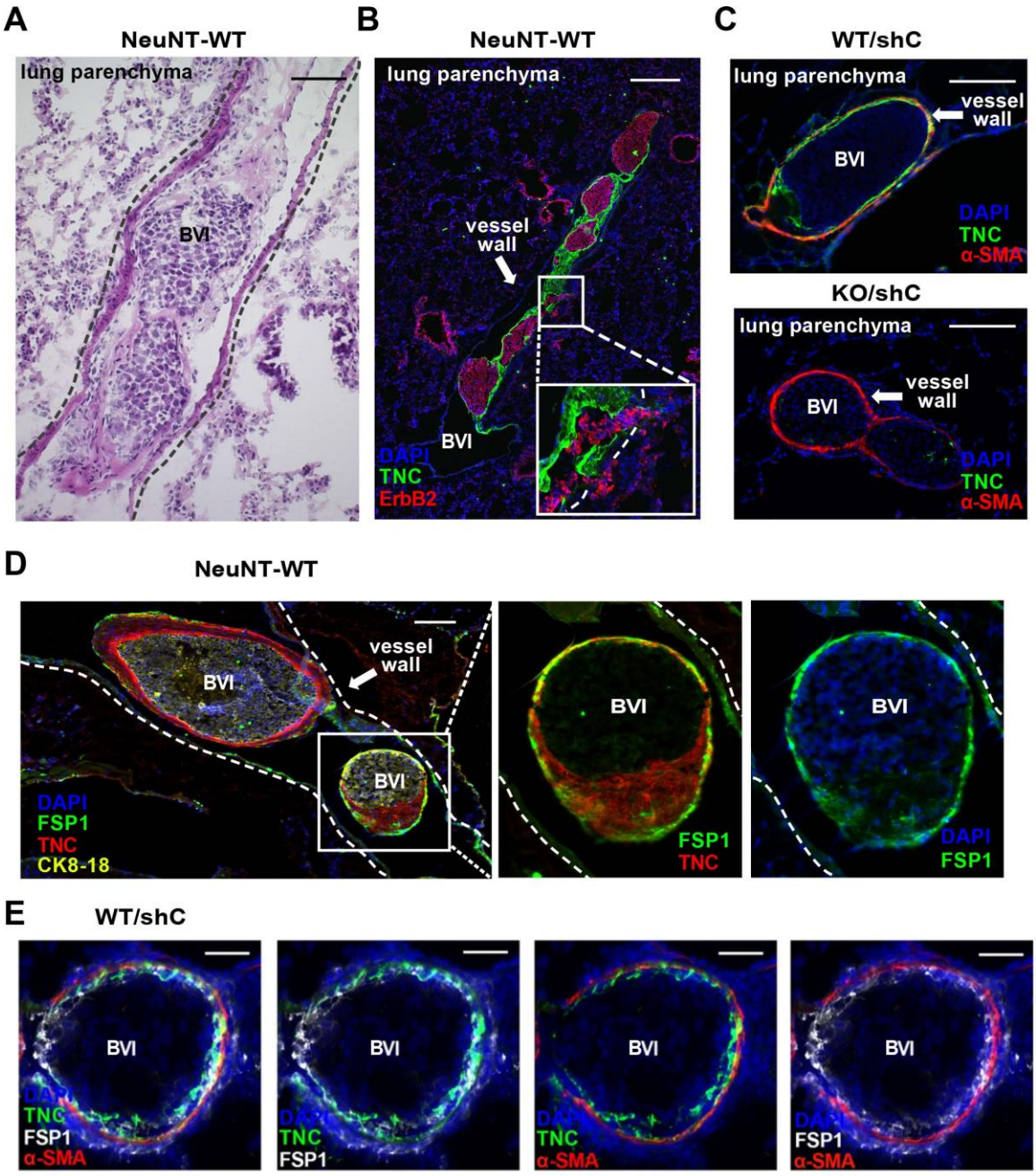

Figure 3. TNC and Fsp1 expression in BVI (A, B) Representative images of BVI in NeuNT-WT lungs upon HE and IF staining for the indicated molecules. **(B)** Note that TNC (green) is expressed around tumor cells (red, ErbB2). Cell nuclei stained with DAPI. Scale bar, 100 µm **(A)**, 500 µm **(B)**. **(C)** Representative IF images for TNC (green) in BVI from WT/shC and KO/shC tumor mice. αSMA staining (red) marks the smooth

muscle/pericyte layer underneath blood vessels. Note, that TNC is expressed in BVI of shC cells engrafted in a WT host, yet not in a TNCKO host indicating that TNC in BVI is of host origin. Scale bar, 100 µm. **(D, E)** Representative IF images for Fsp1+ cells and TNC in BVI from NeuNT-WT **(D)** and WT/shC lung tissue **(E)**. Note overlap of TNC with Fsp1, yet not αSMA, suggesting Fsp1+ cells as a likely source of TNC. Scale bar: 100 µm **(D)**, 50 µm **(E)**. White square represents area of higher magnification.

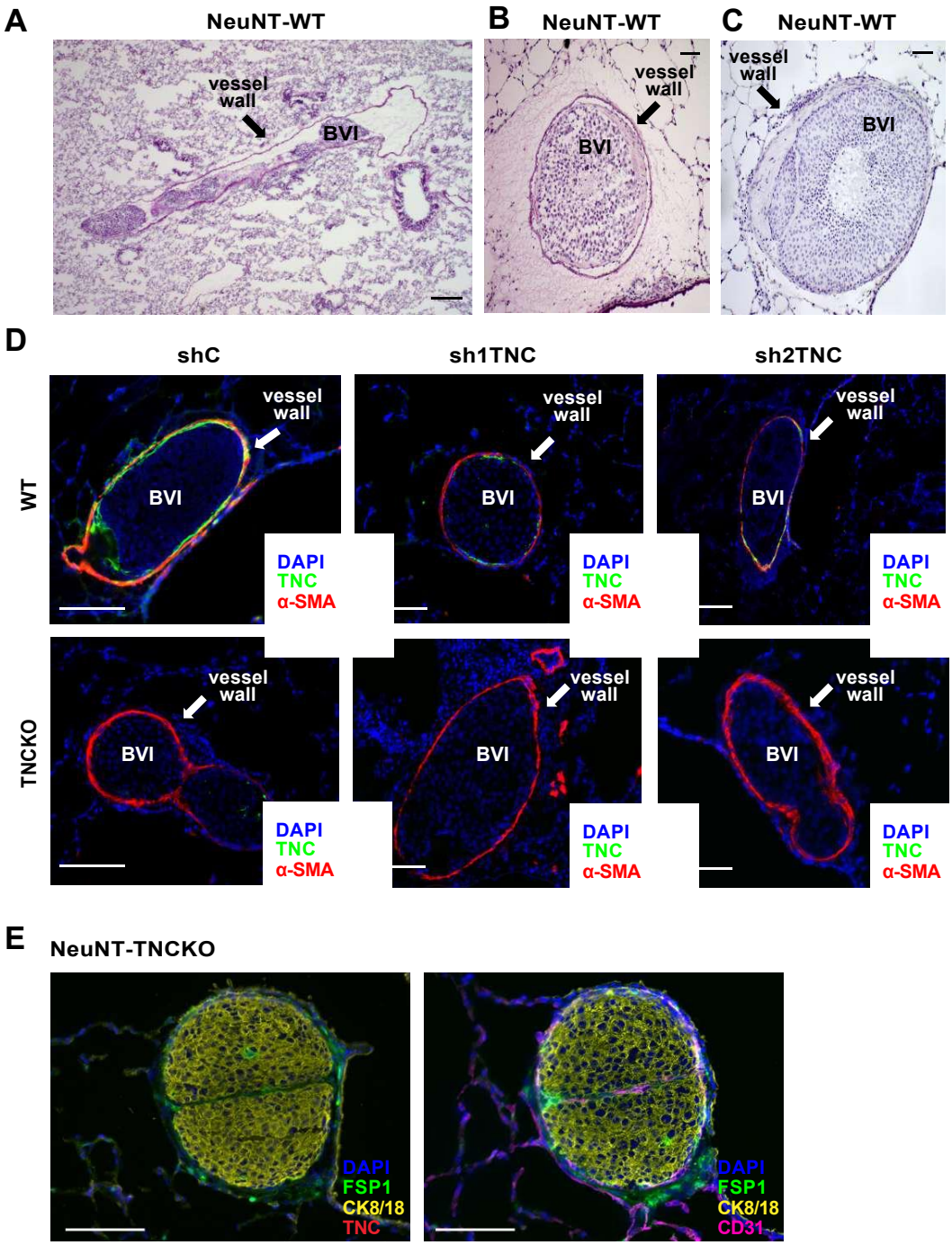
A
NeuNT-WT
vessel wall
BVI
B
NeuNT-WT
vessel wall
BVI
C
NeuNT-WT
vessel wall
BVI
D
shC
sh1TNC
sh2TNC
WT
TNCKO
vessel wall
BVI
DAPI
TNC
α-SMA
E
NeuNT-TNCKO
DAPI
FSP1
CK8/18
TNC
DAPI
FSP1
CK8/18
CD31

Figure S3. Host-derived TNC expression in BVI Representative HE images of BVI in blood vessels of NeuNT-WT **(A - C)**, NeuNT-TNCKO **(E**) and NT193 (**D**) lung tissue. **(B, C)** Note that BVI eventually occlude the vessel lumen and that the central area can be necrotic as indicated by the absence of nucleated cells **(C)**. **(D)** Representative IF images of TNC (green) in BVI from lung tissue derived from NT193 tumor cell grafts. α-SMA staining (red) marks blood vessels. Note, that TNC is expressed when the host expresses TNC (WT/shC) yet not when the host lacks TNC (KO/shC, KO/shTNC). Two images on the left (panel D) are already displayed in Fig. 3C and are shown here again to compare TNC expression between the six conditions. (**E**) Fsp1 expression in BVI of NeuNT-TNCKO mice. Scale bar, 200 µm **(A),** 50 µm **(B, C)** 100 µm **(C, E).**

4. Tenascin-C increases abundance of platelets and integrity of the surrounding endothelial monolayer of BVI

We characterized the cellular and ECM composition of pulmonary BVI of NeuNT-WT mice, by multi-channel immunofluorescence imaging of epithelial/tumor cells (CK8/18, ErbB2), endothelial cells (CD31), platelets (CD41, RAM1), leukocytes (CD45), fibronectin (FN) and laminin (LM) in sequential lung tissue sections. We observed that in all BVI, cancer cells form a tightly packed tumor cell nest that is enveloped by a layer of Fsp1+ cells (**Fig. 3D**). Furthermore, a monolayer of endothelial cells, characterized by flat endothelial cell nuclei, is present at the luminal side of the BVI in the genetic NeuNT-WT (**Fig. 4A, S4A, B)** and the syngeneic NT193 TNC-high (WT/shC) model **(Fig. S4C)**. Moreover, we found distinct layers of LM and FN between the endothelial layer and Fsp1+ cells. Neither FN, LM, TNC nor endothelial cells or fibroblasts were found within the core of the tumor cell cluster (**Fig. 4A**). As plasticity is frequent in cancer and could give rise to cells with mixed tumor and stromal properties [22] we considered that the

Fsp1+ cells may be of tumor cell origin. Yet, we did not see any signal overlap of Fsp1+ with CK8/18, nor ErbB2.

Furthermore, leukocytes (CD45+) were abundant, yet they were not associated with the BVI but were found outside the BVI at the basal side of the vessel wall facing the lung parenchyma (**Fig. 4A, Fig. S4A**). Most interestingly, the layered organization of BVI of the MMTV-NeuNT model is recapitulated in the NT193 grafting model. Again, BVI express a layer of TNC and display a core of proliferating cancer cells and, a layer of fibroblasts and endothelial cells that are separated by FN and LM (**Fig. 3C, E, Fig. S4C**). We investigated the presence of platelets as they are frequently present in circulating tumor cell aggregates and can cause thromboembolism and vessel occlusion [23]. By staining for CD41 or RAM1 (recognizing Gp1b [24]), we found platelets located inside the BVI surrounded by the LM and endothelial layers. This observation suggests a role of platelets early in the evolution of the BVI (**Fig. 4D, S4D-F**). We also noticed an overlap of signals for CD41 and TNC which points at platelets as another potential source of TNC as was previously described in another model [25] (**Fig. S4F**).

Altogether, our detailed analysis revealed the organization of BVI as tightly packed cell clusters (positive for CK8/18 and ErbB2) where some tumor cells are proliferating. Moreover, the nest of tumor cells is enveloped by distinct layers of stromal cells. Whereas Fsp1+ cells, a likely source of TNC, are located adjacent around the tumor cell nest, a layer of endothelial cells is present at the luminal rim of the BVI. Interestingly, the endothelial cells are not in direct contact with TNC but are separated from TNC by other ECM, in particular LM and FN which is consistent with this ECM layer potentially protecting endothelial cells from TNC-induced apoptosis (**Fig. 4F,** [26,27]).

Since BVI are also present in lung vessels of NeuNT-TNCKO mice, we asked whether TNC had any impact on their organization. Staining for LM, FN and Fsp1 did not reveal gross differences between genotypes neither in the transgenic or syngeneic model, suggesting that TNC may not be required for BVI to form (**Fig. 3C, 4B, D**). Besides that, although we observed an endothelial monolayer around BVI in both genotypes (**Fig. 4B, S4A - C**) we noticed more BVI with an intact endothelial layer in NeuNT-WT as compared to NeuNT-TNCKO mice (**Fig. 4B, C**). Interestingly, we also observed an eventual cellular continuum between the endothelial layers of the BVI and the lung vessel wall (**Fig. 4A**). By quantification of CD41 we observed less platelets in pulmonary BVI from NeuNT-TNCKO than NeuNT-WT mice reminiscent of a role of TNC in promoting attachment of platelets, as previously described in a thrombosis model [24] (**Fig. 4D-E**). Overall our data show that, whereas TNC is not required for the formation of pulmonary BVI, stromal TNC has multiple effects on the organization of BVI, promoting endothelial coat integrity, platelet recruitment and tumor cell survival.

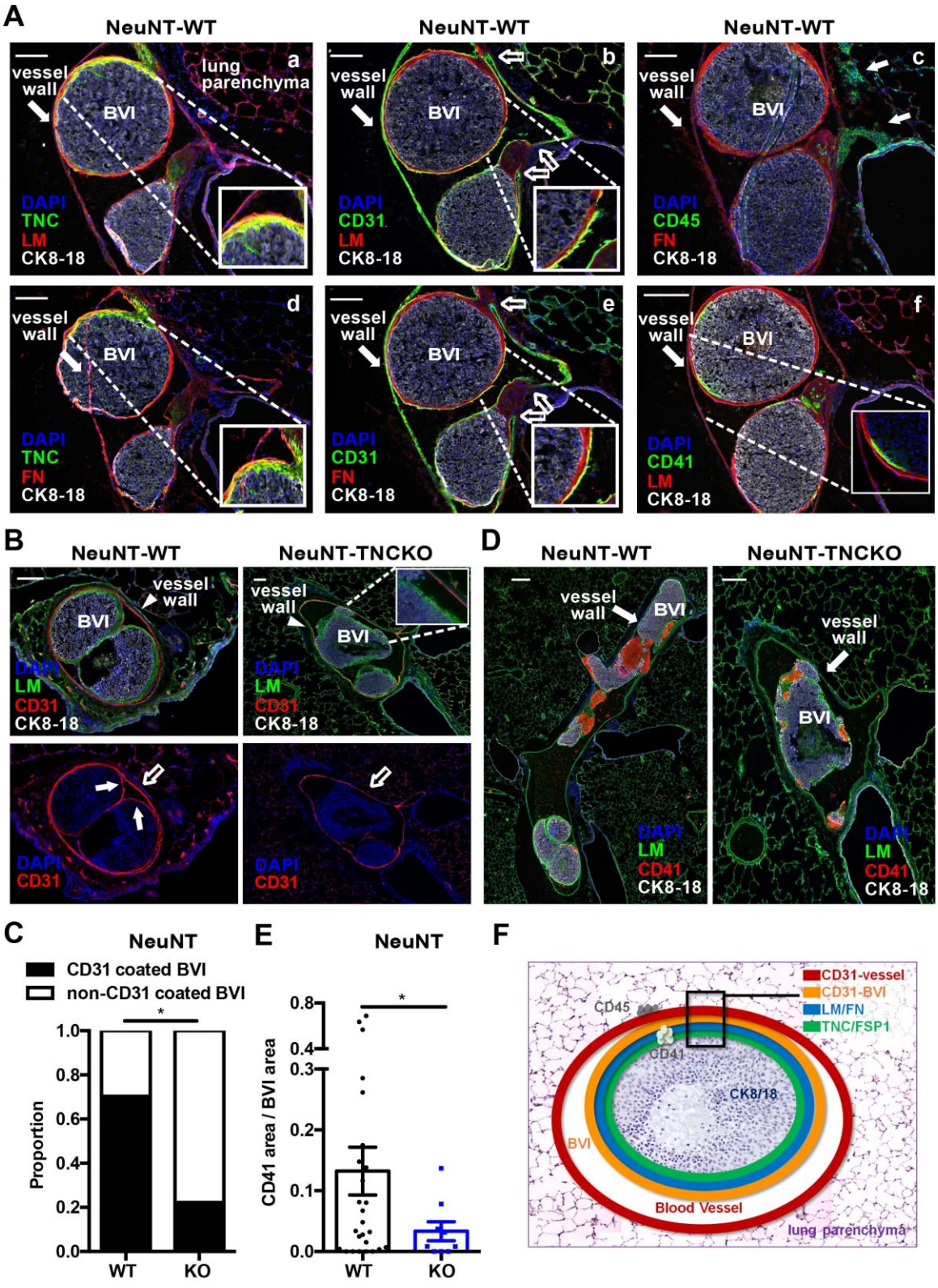
A
NeuNT-WT
NeuNT-WT
NeuNT-WT
vessel wall
BVI
lung parenchyma
a
b
c
d
e
f
DAPI
TNC
LM
CK8-18
DAPI
CD31
LM
CK8-18
DAPI
CD45
FN
CK8-18
DAPI
TNC
FN
CK8-18
DAPI
CD31
FN
CK8-18
DAPI
CD41
LM
CK8-18
B
NeuNT-WT
NeuNT-TNCKO
DAPI
LM
CD31
CK8-18
DAPI
CD31
D
NeuNT-WT
NeuNT-TNCKO
DAPI
LM
CD41
CK8-18
C
NeuNT
CD31 coated BVI
non-CD31 coated BVI
Proportion
WT
KO
E
NeuNT
CD41 area / BVI area
WT
KO
F
CD31-vessel
CD31-BVI
LM/FN
TNC/FSP1
CD45
CD41
CK8/18
BVI
Blood Vessel
lung parenchyma

Figure 4. Cellular organization of BVI (A) Representative images of immunostainings for ECM molecules and cellular markers in BVI of lung tissue from NeuNT-WT (**A, B, D**) and NeuNT-TNCKO mice (**B, D**). The empty arrows point at narrowing of endothelial layers reminiscent of fusion of the endothelial layers derived from the lung vasculature and the BVI. White squares in each panel delineate the field shown at higher magnification. In panel **A**(c) arrows point at CD45+ cells. In panel **A**(d) the vessel staining for FN on the left is an artefact due to disruption of the tissue. Scale bar, 100 µm. **(B)** Representative images of endothelial cells. Arrows point at the endothelial monolayer of the BVI. The empty arrow points at the blood vessel wall. Scale bar, 100 µm. **(C)** Proportion of BVI with and without a CD31 layer for each genotype (NeuNT-WT, N = 6 mice, n = 27 BVI; NeuNT-TNCKO, N = 4 mice, n = 8 BVI). Mean ± SEM, Fisher's exact test. **(D)** Representative images of platelets (CD41+) together with LM. Scale bar, 200 µm. **(E)** Platelet abundance (CD41+ area normalized to area of BVI), NeuNT-WT, N = 6 mice, n = 26 BVI; NeuNT-TNCKO, N = 4 mice, n = 9 BVI. Mean ± SEM, Mann-Whitney test. **(F)** Scheme depicting the composition of BVI. Note, that cancer cells (CK8/18+) are tightly packed inside the BVI, surrounded by Fsp1+ cells, a LM/FN layer and a luminal oriented monolayer of endothelial cells (CD31+). CD45+ leukocytes are not in direct vicinity to the BVI but are present at the basal side of the vessel wall facing the parenchyma. Also, endothelial cells are not in direct contact with TNC.

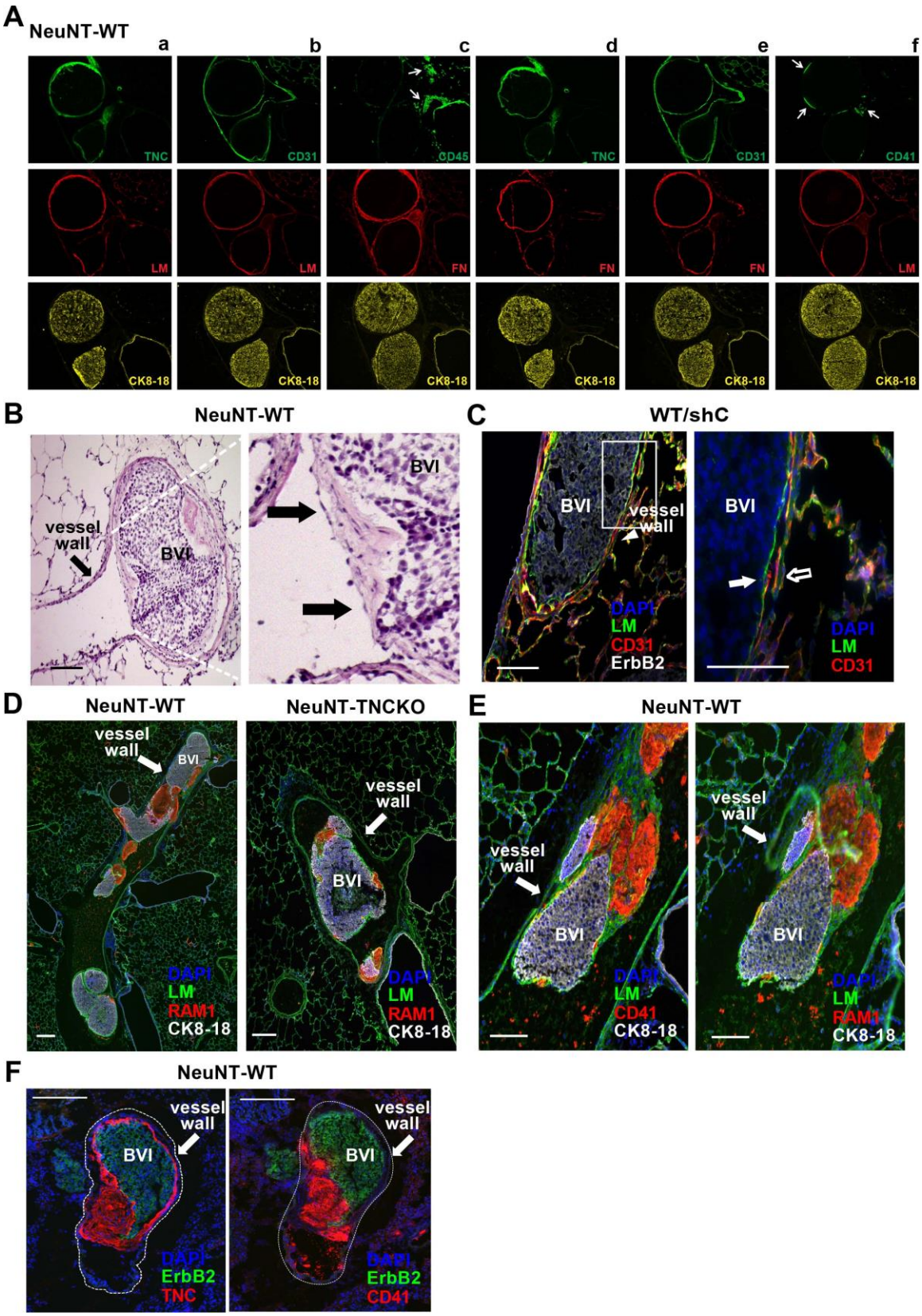
A
NeuNT-WT
a
b
c
d
e
f
TNC
CD31
CD45
TNC
CD31
CD41
LM
LM
FN
FN
FN
LM
CK8-18
CK8-18
CK8-18
CK8-18
CK8-18
CK8-18
B
NeuNT-WT
vessel wall
BVI
BVI
C
WT/shC
BVI
vessel wall
DAPI
LM
CD31
ErbB2
BVI
DAPI
LM
CD31
D
NeuNT-WT
NeuNT-TNCKO
vessel wall
BVI
DAPI
LM
RAM1
CK8-18
vessel wall
BVI
DAPI
LM
RAM1
CK8-18
E
NeuNT-WT
vessel wall
BVI
DAPI
LM
CD41
CK8-18
vessel wall
BVI
DAPI
LM
RAM1
CK8-18
F
NeuNT-WT
vessel wall
BVI
DAPI
ErbB2
TNC
vessel wall
BVI
DAPI
ErbB2
CD41

Figure S4. Presence of endothelial cells and platelets in BVI (A) Separate channels of the IF images shown in Fig. 4A. **(B)** Representative HE images of BVI of NeuNT-WT lung tumor tissue. Note a monolayer of cells with flat nuclei at the luminal border typical for endothelial cells (arrow). A higher magnification is shown in the right panel. Scale bar, 100 µm. **(C)** Representative IF image of endothelial cells (CD31+) in a pulmonary BVI derived from a WT/shC tumor. A higher magnification is shown in the right panel. The filled arrow points at the layer of endothelial cells that surround the BVI, the empty arrow points at a blood vessel. Scale bar, 100 µm. (**D - F**) Representative IF images of platelets (RAM1 (Gp1b), CD41) together with laminin (LM) (**D –** E) or ErbB2 **(F)** in BVI of MMTV-NeuNT mice (WT and TNCKO). Note that platelets and cancer cells are enveloped by a common LM layer indicating an early role of platelets in BVI genesis **(F)**. Scale bar, 200 µm **(C)**, 100 µm **(D, E, F)**.

5.1 Tenascin-C promotes extravasation of tumor cells from pulmonary BVI into the lung parenchyma

We investigated whether BVI are also precursors of parenchymal metastasis in the MMTV-NeuNT model as described in another MMTV-Neu model [17]. Indeed, we observed that the relative abundance of parenchymal metastasis increases over time on account of a reduced number of pulmonary BVI in the MMTV-NeuNT model (**Fig. S5A**). Notably, when we compared the ratio of BVI to parenchymal metastasis we found more parenchymal metastasis than BVI in lungs of NeuNT-WT compared to NeuNT-TNCKO mice (**Fig. 5A**). Similarly, in the NT193 grafting model we saw more parenchymal metastasis in TNC-high than TNC-low conditions (**Fig. 5B**). Interestingly, whereas at the site of extravasation TNC is absent, in the parenchymal metastasis TNC is expressed at the border and in matrix tracks (**Fig. 3B, S5B-E**). Altogether, these results suggest that

TNC plays a role in progression of pulmonary BVI into parenchymal metastasis. TNC also promotes outgrowth of the parenchymal metastasis by promoting survival (**Fig. S1C, D**), similar as seen in a xenograft tail vein injection model [9].

5.2 Tenascin-C increases cellular plasticity in pulmonary BVI and parenchymal metastasis

As pulmonary BVI can act as precursor of parenchymal metastasis, the question arises how tumor cells enter the lung parenchyma. Epithelial-to-mesenchymal-transition (EMT) could be a possible mechanism in the MMTV-NeuNT model as was shown to occur in the MMTV-Neu model [17]. Indeed, in some sections we observed cancer cells leaving pulmonary BVI and invading the parenchymal lung tissue (**Fig. 3B, 4A, 5C**). We investigated the expression of the mesenchymal transition marker vimentin and the epithelial markers CK8/18 and E-cadherin, respectively, in pulmonary BVI. While all tumor cells inside the BVI express CK8/18, E-cadherin and ErbB2, some cells also co-express vimentin (**Fig. 5C, E, S5F, G**). By quantification we noticed more vimentin-expressing cells inside BVI from NeuNT-WT than NeuNT-TNCKO mice (**Fig. 5D, 5E**). Similarly, we also observed vimentin+ cells inside the parenchymal metastasis of NeuNT-WT tissue indicating a mixed epithelial/mesenchymal phenotype (**Fig. S5C, D**). Other cells at the invading front only express vimentin but not E-cadherin, nor CK8/18 or ErbB2 (**Fig. 5C**). A vimentin+ and Ecad+ phenotype is reminiscent of cells undergoing a partial EMT, presumably allowing cells to invade as cell cohorts as has previously reported in another model (MMTV-PyMT, [28] (**Fig. 3B, 5C**). In addition, a mixed tumor cell phenotype in the parenchymal tissue suggests MET that may support tumor cell outgrowth [29].

Altogether, our results suggest that TNC promotes cellular plasticity in pulmonary BVI thereby affecting tumor cell extravasation and outgrowth of parenchymal metastasis.

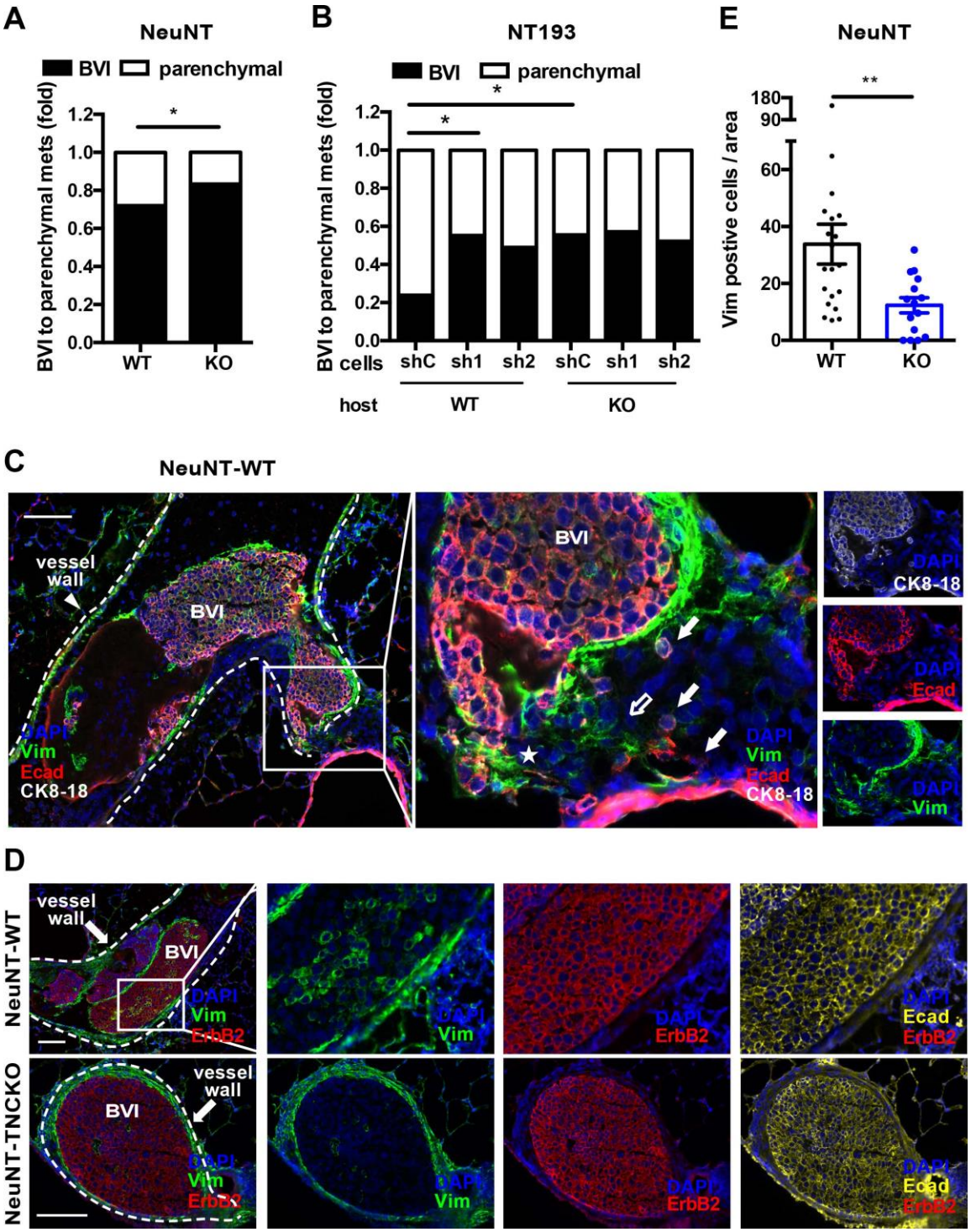

Figure 5. TNC promotes extravasation and plasticity of cancer cells in BVI (A, B) Proportion of BVI to parenchymal metastasis in MMTV-NeuNT mice **(A)** (NeuNT-WT, N = 6 mice; NeuNT-TNCKO, N = 6 mice), $p < 0.02$, Fisher's exact test; and in NT193 grafted mice **(B)** (WT/shC shC, N = 5; WT/sh1TNC, N = 4; WT/sh2TNC, N = 7; KO/shC, N = 6; KO/sh1TNC, N = 5; KO/sh2TNC, N = 5. Mean ± SEM. Chi-square test. Note, that combined TNC expression by the host and the tumor cells increases parenchymal metastasis. **(C, D)** Representative IF images of vimentin (green), E-cadherin (red) and CK8/18 (white) expression in BVI from NeuNT-WT mice. White squares delineate areas of higher magnification. Note, that tumor cells (CK8/18+) are invading the parenchymal lung tissue. Arrow points at single invading tumor cell with epithelial characteristics (CK8/18+ and E-cadherin+). Empty arrow points at invading vimentin+ and E-cadherin- cell. Star points at an event at the invading front. Scale bar, 100 µm. **(E)** Representative IF images of cells expressing vimentin (green), ErbB2 (red) and E-cadherin (yellow) in BVI from NeuNT-WT and NeuNT-TNCKO mice. Scale bar, 100 µm. **(E)** Quantification of tumor cells expressing both vimentin and ErbB2 normalized per BVI area (0.1 mm^2). MMTV-NeuNT (NeuNT-WT, N = 6 mice, n = 20 BVI; NeuNT-TNCKO, N = 4 mice, n = 15 BVI). Mean ± SEM, Mann-Whitney test. Statistical analysis was performed between all groups. Only statistically significant ($p < 0.05$) differences are marked.

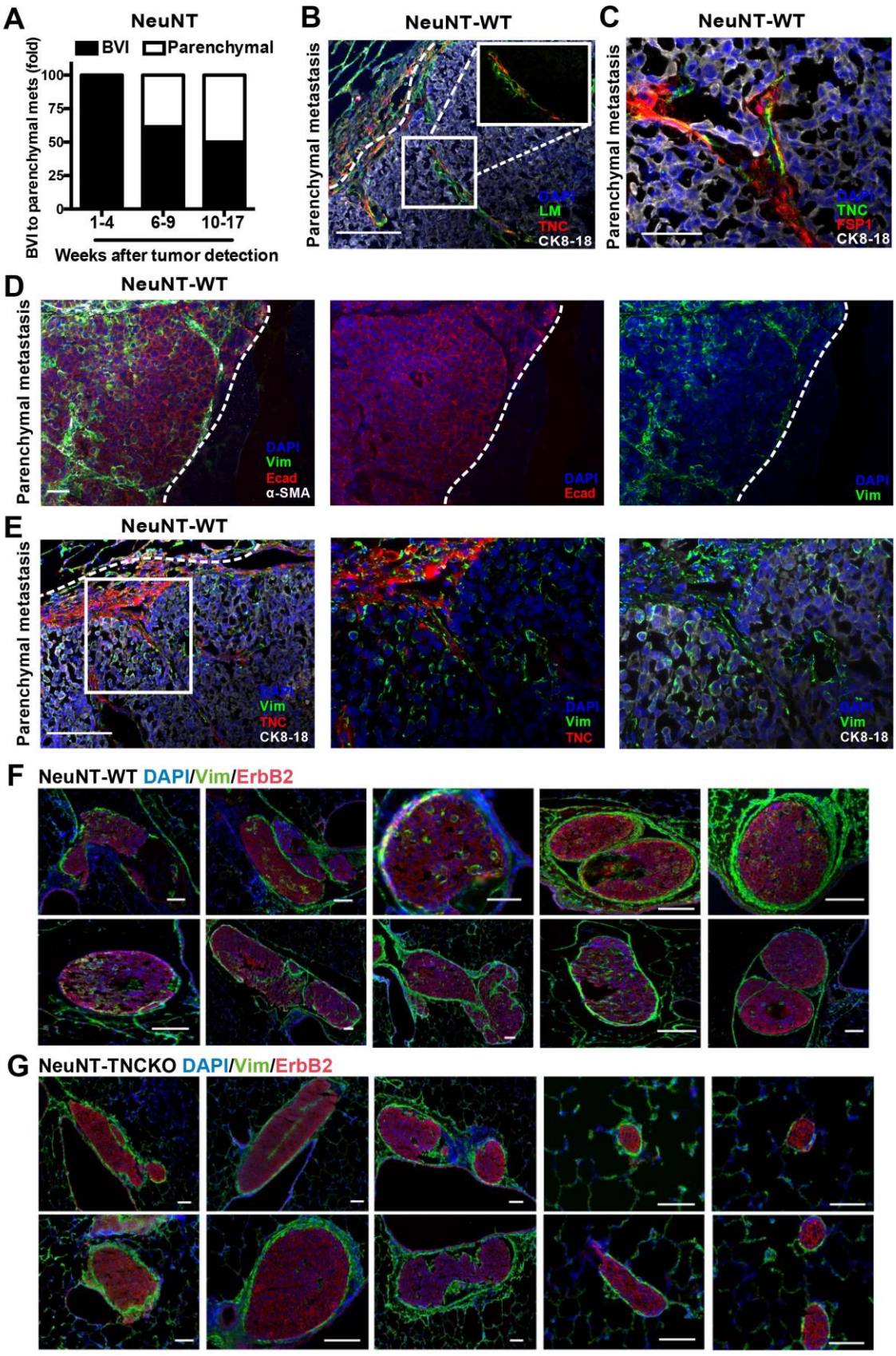
A
NeuNT
BVI
Parenchymal
BVI to parenchymal mets (fold)
100
75
50
25
0
1-4
6-9
10-17
Weeks after tumor detection
B
NeuNT-WT
Parenchymal metastasis
DAPI
LM
TNC
CK8-18
C
NeuNT-WT
Parenchymal metastasis
DAPI
TNC
FSP1
CK8-18
D
NeuNT-WT
Parenchymal metastasis
DAPI
Vim
Ecad
α-SMA
DAPI
Ecad
DAPI
Vim
E
NeuNT-WT
Parenchymal metastasis
DAPI
Vim
TNC
CK8-18
DAPI
Vim
TNC
DAPI
Vim
CK8-18
F
NeuNT-WT DAPI/Vim/ErbB2
G
NeuNT-TNCKO DAPI/Vim/ErbB2

Figure S5. Kinetics of parenchymal lung metastasis and EMT phenotype in parenchymal metastasis and BVI of MMTV-NeuNT mice **(A)** Proportion of BVI and parenchymal lung metastases in MMTV-NeuNT WT mice sacrificed at distinct time points after first tumor detection. 1 - 4 weeks, N = 3 mice with a total of n = 11 BVI; 6 - 9 weeks, N = 3 mice with n = 13 BVI; 10 - 17 weeks, N = 3 mice with n = 10 BVI. **(B-E)** Representative IF images of lung parenchymal metastases of NeuNT-WT mice. White squares delineate fields of higher magnification. **(B)** Note, that TNC (red) and laminin (green) form tracks inside and at the periphery of parenchymal metastases. Scale bar, 100 µm. **(C)** Note that Fsp1 and TNC staining partially overlaps. Scale bar, 50 µm. **(D)** Note, that cells have a mixed phenotype as indicated by expression of E-cadherin and vimentin. Scale bar, 100 µm. **(E)** IF for vimentin and TNC in parenchymal metastasis. Scale bar, 100 µm. **(F, G)** Representative IF images of vimentin+ (green) and ErbB2+ (red) cells in BVI of lung tissue from NeuNT-WT (N = 6 mice, n = 20 BVI) **(F)** and NeuNT-TNCKO mice (N = 4 mice, n = 15 BVI) **(G)**. Note, that cells that express ErbB2 also express E-cadherin and CK8/18 indicating their epithelial characteristics. Scale bar, 100 µm.

6. Tenascin-C induces EMT in cultured tumor cells, promoting cell migration and survival through TGF-β signaling

TNC has been shown to induce an EMT-like phenotype in conjunction with TGF-β in cellular models [30,31]. Therefore, we asked whether TNC induces EMT in NT193 cells. We added purified TNC to NT193 cells grown as monolayer or as spheroid cultures and indeed observed EMT as indicated by loss of E-cadherin and gain of vimentin expression as demonstrated by immunofluorescence imaging, quantitative reverse transcription PCR (qPCR) and immunoblotting (**Fig. 6A - C**). Moreover, we noticed increased mRNA levels

of several other EMT markers, such as *Snail*, *Slug*, *Zeb1*, *Pai-1*, *Mmp9* and *Tnc* itself upon treatment with TNC. On the contrary, mRNA levels of *E-cadherin* were found reduced (**Fig. 6B**).

Next, we compared cell responses to TNC with that to TGF-β and, found that similar to TNC, TGF-β induces an EMT in NT193 cells as evidenced by loss of E-cadherin and gain of vimentin expression (**Fig. 6A-C, Fig. S6A, B**). Notably, the TGF-β signaling inhibitor GW788388 (GW) reverts the TNC-induced mesenchymal phenotype into an epithelial one, as expression of E-cadherin is increased and that of vimentin is decreased (**Fig. 6A – C, Fig. S6A, B**). These results demonstrate that TNC induces EMT in NT193 cells through TGF-β signaling.

We determined downstream signaling upon TNC treatment by immunoblotting and observed that in addition to phosphorylated Smad (p-Smad2) also levels of p-Akt and p-Erk1/2 increase, suggesting an induction of both canonical and non-canonical TGF-β signaling by TNC. Moreover, all three of the TNC-induced signaling pathways are TGF-β dependent as they were blocked with GW (**Fig. 6C, S6B**).

As we observed platelets residing inside the pulmonary BVI and platelets are known to induce an EMT [25], we considered a potential role of platelets in EMT in our models. Indeed, in cultured cells, we found that platelets induce an EMT, since E-cadherin levels are decreased and vimentin expression is increased. Similar to TNC, also the platelet-induced EMT was blocked with GW, suggesting that a platelet-induced EMT is TGF-β signaling-dependent in NT193 cells (**Fig. 6D**).

Next, we asked what consequences a TNC-induced TGF-β-dependent EMT has for the cells. We used a cellular wound closure assay and observed increased migration of cells upon addition of TNC, which was comparable to the treatment with TGF-β (**Fig. 6E, F**).

Again, this effect was blocked with GW indicating that TNC-induced EMT increases NT193 cell motility through TGF-β signaling.

Since EMT provides tumor cells with survival resistance against toxic reagents [32], we next determined staurosporine-induced apoptosis by a caspase-3/7 activity assay and observed that pre-treatment of NT193 cells with TNC for 24 hours reduces apoptosis. The TNC effect was similar to that of TGF-β and was reverted by GW, suggesting that a TNC-induced EMT protects against apoptosis where TGF-β signaling is important (**Fig. 6G, Fig. S6D**).

Next we investigated how TNC activates the TGF-β signaling pathway. Since TNC was shown to bind TGF-β [33], we investigated by ELISA whether our TNC preparations potentially contained TGF-β. Yet no TGF-β was found (**Fig. 6H**). We further determined whether cells potentially secrete more TGF-β upon treatment with TNC. Therefore, we added TNC to TNC-devoid NT193 sh2TNC cells (**Fig. S2A**) and, compared TGF-β secretion to cells that have been treated with TGF-β. Indeed, cells express more TGF-β upon treatment with TNC similar to levels detected in cells that were treated with TGF-β itself. This was not the case for the recombinant TNC domain molecule TNC-FGB (fibrinogen globe) and, TNC-FnIII3-5 (fibronectin type III repeat 3-5) that was described to bind TGF-β [33], despite 10-fold higher molarity than TNC (**Fig. 6H**).

Investigating the kinetics of canonical (Smad) and non-canonical (Akt, Erk1/2) TGF-β signaling [34], revealed rapid signaling activation by TNC which paralleled that of TGF-β itself and may contribute to enhanced survival by TNC. Phosphorylated Smad2 peaked around 2 hours and was increased at 24 hours comparable to the kinetics of p-Akt and p-Erk1/2. Levels of E-cadherin and vimentin started to drop and rise, respectively, upon addition of TNC similar to the treatment with TGF-β (**Fig. S6E, F**).

In conclusion, our results have shown that in NT193 cells TNC activates canonical and non-canonical TGF-β signaling with a similar kinetic as TGF-β itself, leading to increased abundance of TGF-β in the cell supernatant. How TNC increases TGF-β levels and induces TGF-β signaling remains to be determined. Importantly, our study revealed an instrumental role of TNC in inducing EMT in our cellular system and, in the pulmonary BVI.

As TGF-β signaling promoted metastasis in a MMTV-Neu model [17] induction of TGF-β signaling could explain cellular plasticity and progression of BVI into parenchymal metastasis, thus elevating total metastasis burden in MMTV-NeuNT mice. A similar mechanism as recently demonstrated for fibronectin fibrils to activate TGF-β signaling should be investigated for TNC in the future [35].

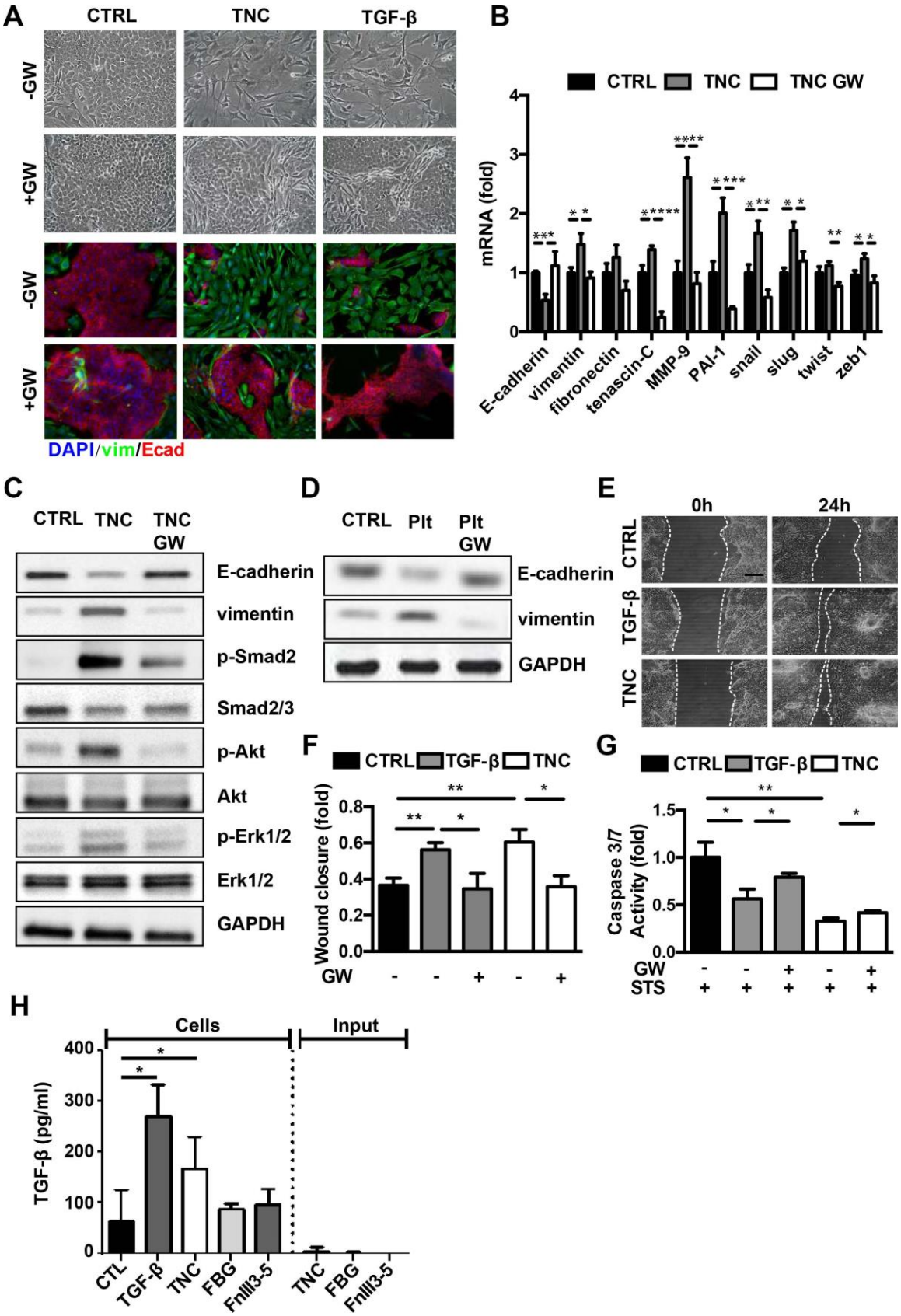
A
CTRL
TNC
TGF-β
-GW
+GW
-GW
+GW
DAPI/vim/Ecad
B
CTRL
TNC
TNC GW
mRNA (fold)
E-cadherin
vimentin
fibronectin
tenascin-C
MMP-9
PAI-1
snail
slug
twist
zeb1
C
CTRL
TNC
TNC GW
E-cadherin
vimentin
p-Smad2
Smad2/3
p-Akt
Akt
p-Erk1/2
Erk1/2
GAPDH
D
CTRL
Plt
Plt GW
E-cadherin
vimentin
GAPDH
E
0h
24h
CTRL
TGF-β
TNC
F
CTRL
TGF-β
TNC
Wound closure (fold)
GW
G
CTRL
TGF-β
TNC
Caspase 3/7 Activity (fold)
GW
STS
H
Cells
Input
TGF-β (pg/ml)
CTL
TGF-β
TNC
FBG
FnIII3-5
TNC
FBG
FnIII3-5

Figure 6. In cultured NT193 cells TNC induces EMT promoting cell migration and survival (A) Phase contrast micrographs and IF images of E-cadherin (red) and vimentin (green) stained NT193 cells treated with TGF-βR1 inhibitor (GW788388) prior to addition of TNC and TGF-β for 24h, respectively. Nuclei stained by DAPI. Scale bar, 20 μm. **(B)** Relative expression (fold change) of the indicated genes in NT193 cells upon treatment with GW788388 and TNC for 24 hours (n = 5, five independent experiments) with normalization to GAPDH. **(C)** Detection of E-cadherin, vimentin, phosphorylated pathway markers (Smad2, Akt, and Erk1/2), respectively and expression of total markers (Smad2/3, Akt, Erk1/2) by immunoblotting with GAPDH as loading control (a representative of three independent experiments is shown). **(D)** Detection of E-cadherin and vimentin expression by immunoblotting of lysates from NT193 cells upon addition of platelets for 24 hours (n = 3, three independent experiments). **(E, F)** Wound closure of NT193 cells, n = 14, five independent experiments with at least two replicates. Scale bar, 20 μm. **(G)** Assessment of staurosporine (STS) - induced apoptosis by measuring caspase-3/7 activity in NT193 cells treated as indicated, n = 9, three independent experiments in triplicates. **(H)** Quantification of TGF-β released by NT193 cells upon treatment with TNC, TNC-FBG and TNC-FnIII3-5 by ELISA. Note that purified TNC and recombinant TNC domain molecules are free of TGF-β. **B, F, G, H,** Mean ± SEM, unpaired Student t test. Statistical analysis was performed between all groups. Only statistically significant ($p < 0.05$) differences are marked.

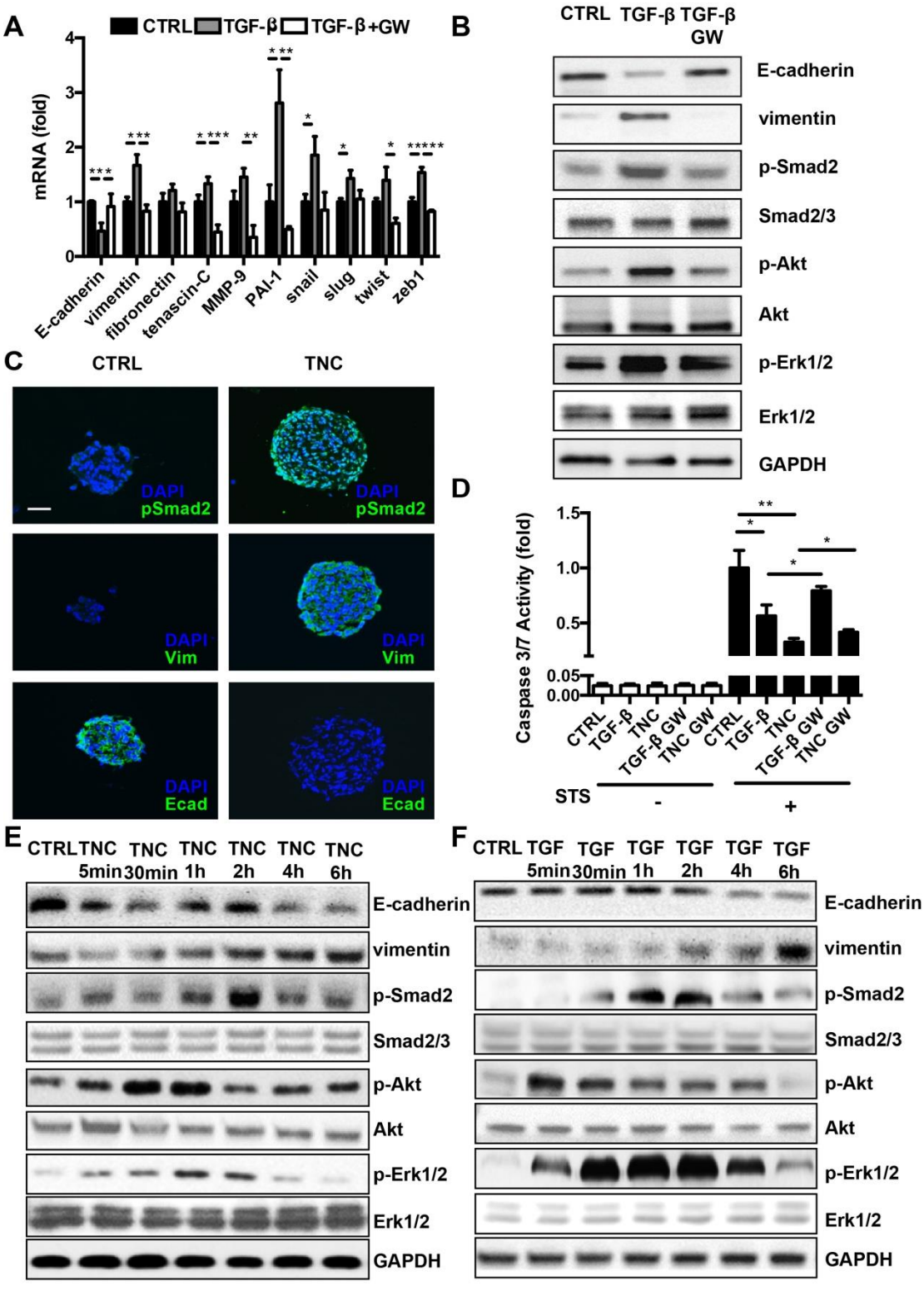
A
CTRL
TGF-β
TGF-β+GW
mRNA (fold)
E-cadherin
vimentin
fibronectin
tenascin-C
MMP-9
PAI-1
snail
slug
twist
zeb1
B
CTRL
TGF-β
TGF-β GW
E-cadherin
vimentin
p-Smad2
Smad2/3
p-Akt
Akt
p-Erk1/2
Erk1/2
GAPDH
C
CTRL
TNC
DAPI
pSmad2
DAPI
Vim
DAPI
Ecad
D
Caspase 3/7 Activity (fold)
CTRL
TGF-β
TNC
TGF-β GW
TNC GW
STS
-
+
E
CTRL
TNC 5min
TNC 30min
TNC 1h
TNC 2h
TNC 4h
TNC 6h
E-cadherin
vimentin
p-Smad2
Smad2/3
p-Akt
Akt
p-Erk1/2
Erk1/2
GAPDH
F
CTRL
TGF 5min
TGF 30min
TGF 1h
TGF 2h
TGF 4h
TGF 6h
E-cadherin
vimentin
p-Smad2
Smad2/3
p-Akt
Akt
p-Erk1/2
Erk1/2
GAPDH

Figure S6. Role of TGF-β and TNC on EMT and cell behaviour in cultured NT193 cells **(A)** mRNA expression levels of the indicated genes (fold change) in NT193 cells upon treatment with TGF-βR1 inhibitor (GW788388) and TGF-β for 24 hours (n = 5, five independent experiments). Normalization to GAPDH. **(B)** Detection of E-cadherin, vimentin, phosphorylated Smad2, Akt, and Erk1/2, respectively and total Smad2/3, Akt, Erk1/2 by immunoblotting of lysates from NT193 cells treated as indicated. GAPDH was used as loading control (n = 3, three independent experiments). **(C)** IF images of E-cadherin, vimentin and phospho-Smad2/3 (green) of NT193 spheroids upon treatment with TNC. Cell nuclei stained with DAPI. Scale bar, 20 µm. **(D)** Assessment of staurosporine (STS)-induced apoptosis by measuring caspase-3/7 activity in NT193 cells treated as indicated, n = 9, three independent experiments in triplicates. Note, that results shown in Fig. 6G are presented together with all controls. **(E, F)** Kinetics of expression of the indicated molecules in NT193 cells upon addition of TNC (**E**) and TGFβ (**F**) for the indicated time points assessed by immunoblotting. GAPDH was used as loading control (n = 3, three independent experiments). **A, D,** Mean ± SEM, unpaired Student t test. Statistical analysis was performed between all groups. Only statistically significant ($p < 0.05$) differences are marked.

7. Tenascin-C is expressed in BVI from human carcinomas yet not in LVI

Vascular invasions in the primary tumor comprise an important prognostic tool and can occur in blood and lymphatic vessels [36,37]. To address whether BVI and LVI of human carcinomas express TNC, we investigated tissue from several human carcinomas with and without recorded presence of vessel invasions by sequential staining for TNC, CD31, podoplanin and platelet marker CD61 (**Table 1, S3, S4**). We observed BVI (tumor cell clusters inside CD31+ vessels) and LVI (tumor cell clusters inside D2-40+ vessels). In

particular, we saw BVI in a total of 23 tumors comprising renal cell carcinoma (RCC), hepatocellular carcinoma (HCC) and pancreatic neuroendocrine tumors (PNET)) and, LVI in a total of 47 cases comprising pancreatic adenocarcinomas (PDAC (7 cases)) and mammary carcinomas (MaCa (40 cases)) (**Fig. 7A-C, S7**, **Fig. S8, Table 1**). Although we do not have evidence for a simultaneous existence of BVI and LVI in the same tumor this possibility cannot be ruled out. As in the MMTV-NeuNT model, we noted that BVI are surrounded by a luminal endothelial monolayer and a TNC layer. When BVI were bigger, TNC and endothelial cells were also detected inside the BVI (**Fig. 7A, C, S7A, B and C**). By contrast, LVI were neither covered by an endothelial cell layer nor did they express TNC (**Fig. S8A, B, Table 1**). Interestingly, tumor cell aggregates were present in lymphatic vessels (LVI) in MaCa independently of the subtype and appeared mostly as smaller floating cell clusters (**Fig. S8B, Table 1**). Upon an unbiased search in MaCa and the corresponding lung metastases we observed only LVI.

To our knowledge, these results demonstrate for the first time differences in cellular content and matrix composition between BVI and LVI. As in the murine metastatic models, in human cancers, BVI are enclosed by an endothelial monolayer and, express TNC.

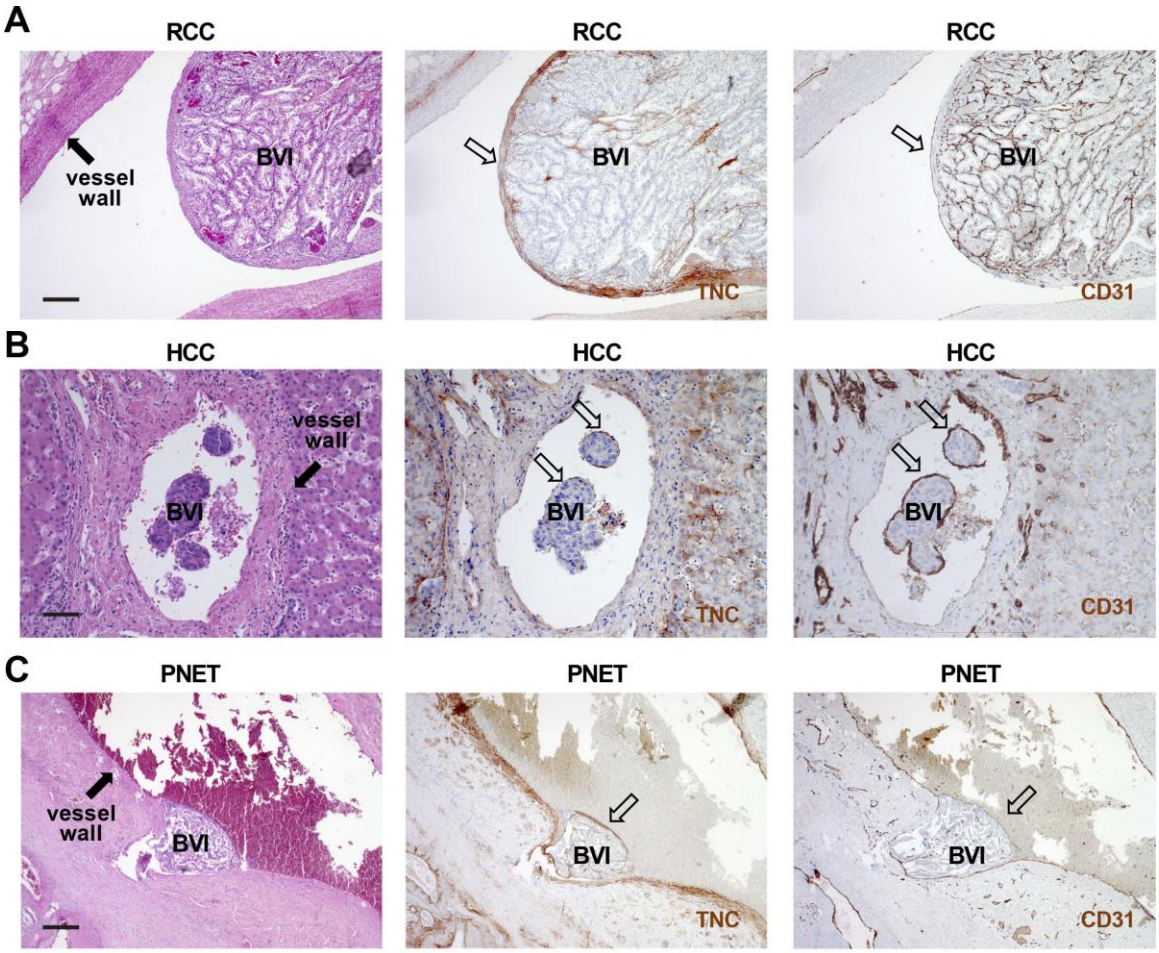

Figure 7 BVI of human cancers are surrounded by endothelial cells and TNC Consecutive tissue sections from human RCC, HCC and PNET were stained for H&E, CD31 and TNC. Representative images are shown. Note, that BVI are surrounded by a luminal endothelial monolayer and express TNC beneath the endothelial layer (open arrows). Note, that tumor cell clusters were found to protrude into the lumen of blood vessels (filled arrows), in particular the renal veins (RCC), the portal vein and branches of the portal vein (HCC) and the stem or branches of the superior mesenteric vein (PNET). In PNET a thrombotic reaction is observed at the luminal surface of the endothelium covering the BVI (arrow). Scale bar, 50 μm.

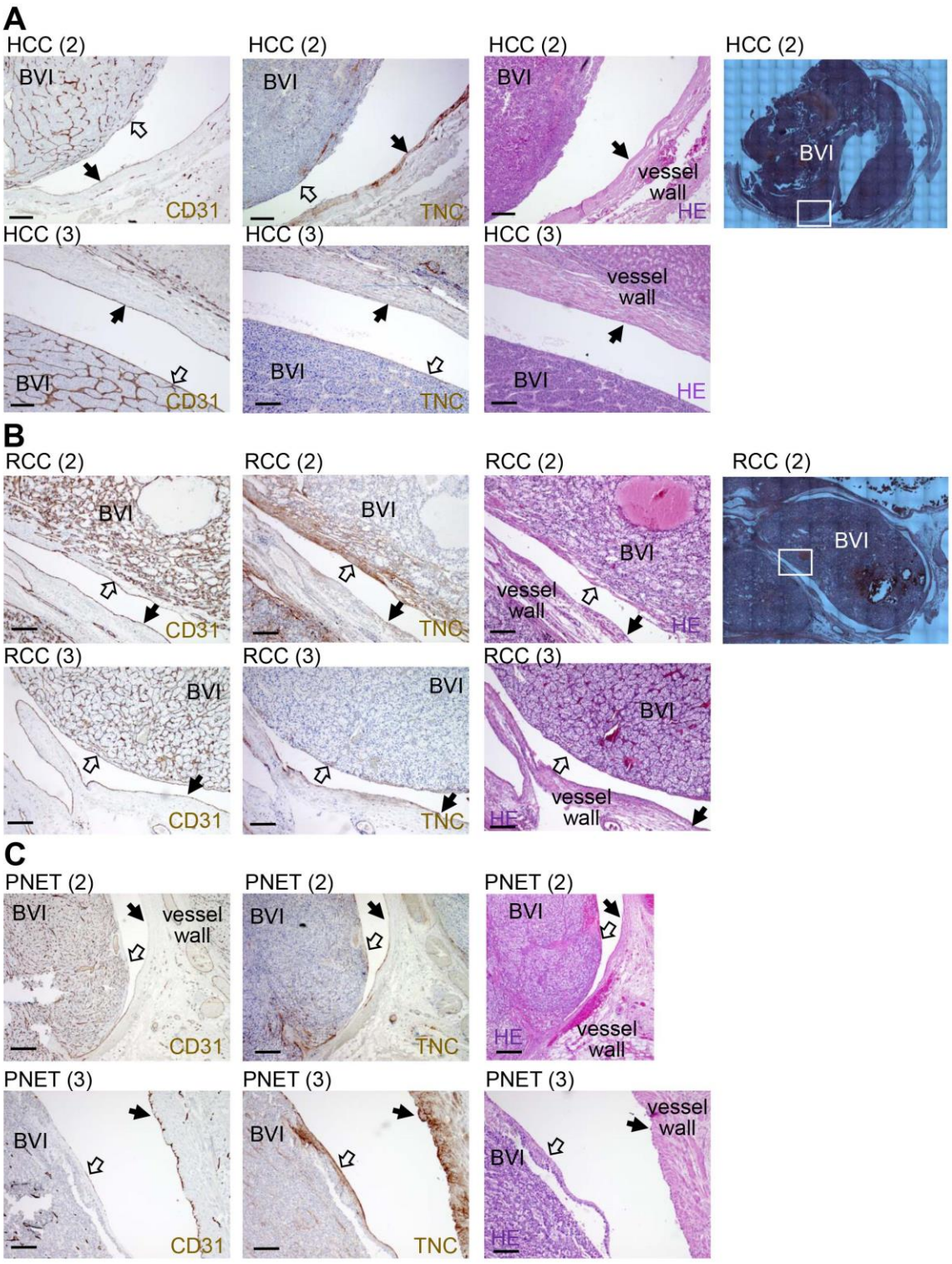

Figure S7 BVI in human cancer are characterized by endothelial cells and TNC expression Consecutive tissue sections from human RCC, HCC and PNET were stained

for HE, CD31 and TNC. Representative images including mosaic images (upper image in A and B) are shown that demonstrate almost filling of the invaded veins by the BVI (filled arrows). Note that BVI are surrounded by a luminal endothelial monolayer and express TNC beneath the endothelial layer (open arrows). Scale bar, 50 μm.

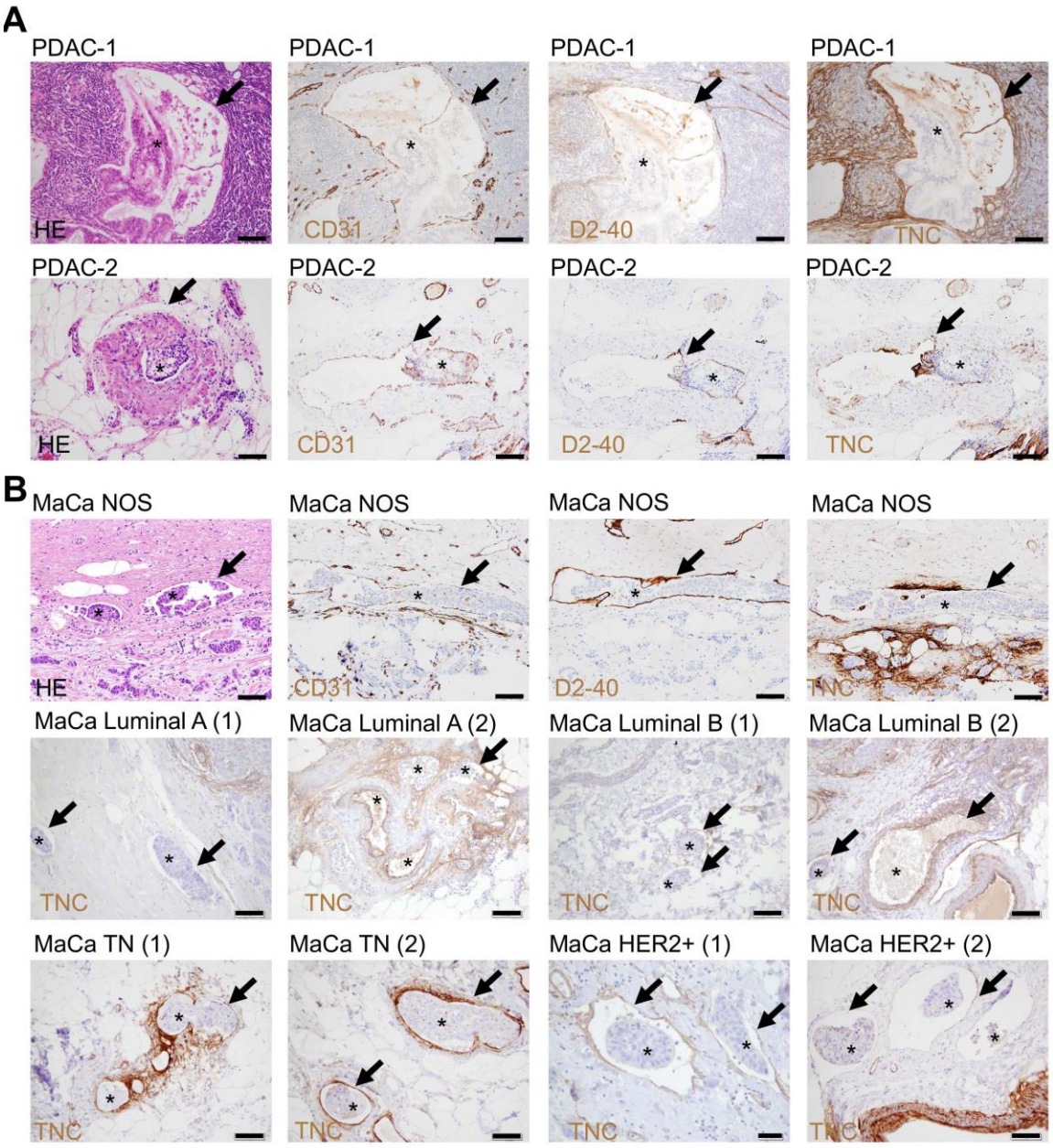

Figure S8 LVI in MaCa and PDAC Representative images of human invasive PDAC (**A**) and invasive MaCa (**B**) are shown upon staining with HE or antibodies specific for endothelial cells (CD31), lymphatic vessels (D2-40) and TNC, respectively. Arrow points at infiltrated lymphatic vessel. LVI are marked with a star. Note, that LVI are not enveloped by an endothelial monolayer, nor do they express TNC. In contrast the lymphatic vessel or the surrounding tissue can abundantly express TNC. Scale bar, 20

μm (Her2+ (1), TN (2)), 50 μm (PDAC (1), Luminal A (1/2), Luminal B (1/2), TN (1), Her2+ (2)), 100 μm (PDAC (2), MaCa).

Discussion

It is well established that the ECM plays an important role in tissue homeostasis enhancing pathologies including tumor malignancy and metastasis [7,38,39]. Moreover, the ECM molecule TNC which is abundantly expressed in cancer tissue enhances metastasis [9–11,40], yet by incompletely understood mechanisms. To address the roles of TNC in metastasis, we have compared NeuNT (ErbB2)-driven lung metastasis in a genetic and a novel syngeneic orthotopic breast cancer model derived thereof with high TNC to that with no or low TNC, respectively. Of note ErbB2-driven models may not well recapitulate human breast cancer metastasis where LVI are frequent, but better phenocopy cancer progression of other tumors that develop BVI in blood vessels of the lung [16,17]. Our results reveal the cellular and molecular characteristics of BVI, offering future targeting opportunities. We further elucidate multiple novel functions of host-derived TNC in progression from pulmonary BVI into parenchymal metastasis that were unknown so far.

We report that pulmonary BVI are organized as clusters of proliferating epithelial tumor cells with tight junctions. Tumor cell cohesion may contribute to synoikis, a recently identified survival mechanism with relevance for targeting [41][2]. Tumor cell nests are enveloped by a luminal endothelial cell monolayer and Fsp1+ cells, also a likely source of TNC in this model [21]. FN and LM are expressed between the two stromal cell layers (**Fig. 4**). Thus targeting tumor cell cohesions in BVI, endothelial cells or TNC expression itself (e.g. by Fsp1+ cells) could represent novel strategies. This could complement already identified inhibition of ErbB2 (MMTV-NeuNT) [20] and TGF-β signaling (MMTV-Neu NDL) [17] in reducing metastasis in these models.

It is interesting to note that in the MMTV-NeuNT model TNC induces a partial EMT where TGFβ signaling may play a decisive role as we observed that TNC induces EMT in cultured tumor cells in a TGFβ dependent manner. That only some tumor cells within the BVI as well as at the rim and site of extravasation, that are not necessarily in direct contact with TNC, have gained expression of the EMT marker vimentin, is intriguing to note and suggests a paracrine effect through which TNC impacts EMT in the BVI. In vitro, TNC-induced EMT enhances migration and survival of tumor cells which may also apply in the BVI. As TGFβ signaling plays a role in promoting cancer stemness properties and survival in another model [42], future research has to clarify whether TNC also impacts cancer stemness through TGFβ signaling in this model.

Due to lack of appropriate models, until now it was difficult to assign the cellular source of TNC with a function. Grafting human tumor cells with engineered TNC levels in the tail vein of immune compromised mice previously showed that tumor cell-derived TNC is relevant in early stages of lung colonization [9] but how host TNC affects spontaneous metastasis in immune competent conditions was unknown. Now, by using our novel orthotopic immune competent transplantation model with engineered TNC levels and spontaneous metastasis and, kinetics that generate a relevant TME, we showed for the first time that host-derived TNC plays a crucial role in metastasis, before tumor cell breaching. This could be relevant for future targeting as it may not suffice to kill tumor cells, but also to target stromal cells expressing TNC.

Several concepts for the formation of BVI and their endothelialization exist, as e.g. transdifferentiation of tumor cells into endothelial cells [36], budding of tumor cells from the primary tumor [43], recruitment of bone marrow-derived endothelial progenitor cells

(EPC) [44] and, endothelialization [3], where endothelial cells and TNC are active participants. In a model proposed by Sugino et al., (2002) clusters of cancer cells in the primary tumor enter the circulation through an invasion-independent pathway, form local BVI and eventually migrate until they reach the site of metastasis [43]. Notably, the size of some of the BVI in this study suggests that, if circulating BVIs existed in their model, they would be present in large vessels. Another model suggests that single cells or clusters of circulating tumor cells (CTC), with or without an ECM coating and stromal cells, proliferate in the lung vasculature forming BVI at the metastatic site. Several observations support this model. Clusters of around 50 CTC were identified in tumor-bearing mice and, represent a higher metastatic potential than single CTC [45]. Moreover, a few hours after tail vein inoculation, cancer cells found in the lumen of lung vessels were already coated with ECM and platelets. These authors suggest that BVI formation occurs when cancer cells reach pulmonary arterioles but not capillaries [3]. Here, we show that stromal cells, probably platelets or Fsp1+ cells, are a source of TNC in pulmonary BVI. The prominent location of platelets deep inside the BVI (our observation) argues for an early role of platelets in BVI formation, apparently immediately after intravasation [25]. Finally, stromal cells on pulmonary BVI can migrate from the primary tumor as proposed in another model [46].

We consider the trans-differentiation of tumor cells into endothelial cells [28] as unlikely, since endothelial cells form a contiguous monolayer and are not found inside the BVI core. Also, budding from the tumor vasculature [27] may not occur as we do not see a monolayer of αSMA+ cells underneath the endothelial layer in the BVI. Upon release into the circulation by budding, only tumor cells at the periphery of the tumor cell cluster would get in contact with platelets and therefore platelets should be placed at the rim of the BVI.

Yet, this is not the case, as we see platelets inside the BVI beneath the endothelial layer. On the contrary, we consider endothelialization, where endothelial cells from the vasculature wrap around circulating tumor cells [3], a likely scenario, as we observed a mostly contiguous monolayer of endothelial cells around the BVI, in the murine model and in human cancers, occuring in the primary tumor as well as in the metastastic lung.

As in the MMTV-NeuNT model also in MMTV-NeuYD mice endothelialization of BVI is frequent, yet only when VEGFA is coexpressed (MMTV-NeuYD/VEGFA) [47]. Also, VEGFA was involved in TNC-promoted lung metastasis in the 4T1 grafting model establishing a crosstalk of TNC with endothelial cells in metastasis [21]. As VEGFA can bind to TNC, a potential combined impact on endothelial cells is likely [11]. We showed that BVI endothelial layer integrity, tumor cell survival and overall metastasis were correlated and, promoted by TNC. Thus, it is conceivable that impacting BVI endothelialization is an important mechanism how TNC promotes metastasis. Given its role in promoting the angiogenic switch and tumor angiogenesis [11,26,27,48] future research has to determine how TNC impacts BVI endothelial cell function and endothelialization. This may involve an autocrine mechanism as previously described, where TNC induced Wnt signaling, VEGFA and a pericellular fibronectin layer in endothelial cells [11,27]. Also a paracrine mechanism may apply where TNC induces pro-angiogenic factors in tumor cells, fibroblasts or Fsp1+ cells as previously described in other tumors [21,26]. In this scenario, TNC-induced TGFβ signaling could play a role in promoting survival of endothelial cells of the BVI.

Lympho-vascular invasions are frequently observed in routine analysis of many cancers, but incidence and relevance depends on the tumor type and subtype [49–52]. By using

blood- and lymph-vessel markers recent analysis allowed to discriminate between LVI and BVI. Whereas LVI appeared smaller in size and in smaller vessels, many BVI were huge and present in bigger vessels (our results). Maybe physical properties such as local high shear stress in bigger vessels impacts the size of BVI which has to be addressed in the future. So far there are only a dozen of retrospective studies that analyzed the impact of BVI versus LVI in cancer. BVI can be found inside and in the periphery of primary breast tumors, but apparently in breast cancer BVI are less frequent than LVI [5,49,53–55].

A few studies analyzed the relevance of tumor BVI versus LVI as a prognosis factor in breast cancer, but the results are controversial [5,53–55]. Disseminated lympho-vascular invasions are almost impossible to identify ante mortem [56]. Here our models could be highly relevant as both, the MMTV-NeuNT and the autochthonous grafting model that we had developed, present intra- and peritumoral BVI and, more importantly, disseminated BVI in the lung. Clinical trials of anti-angiogenic drugs failed to improve recurrence-free survival of breast cancer patients and lost approval by the FDA [57–59]. However, the presence of BVI/LVI was not considered as an inclusion factor. We believe that anti-angiogenic drugs can impair disseminated BVI, decrease metastasis and increase survival of breast cancer patients with BVI. Since BVI are frequent in many tumors and have an endothelial lining they may respond to anti-angiogeneic drugs, which has to be addressed in the future. Indeed impacting the endothelial layer of BVI may reduce metastasis, as our results from the TNCKO mice suggest, where we observed an interrupted or missing endothelial BVI monolayer and, reduced overall metastasis in the absence of TNC. Anti-angiogenic drug treatment is already applied in patients with RCC, HCC and PNET [60] thus, likely affecting BVI. Hence, TNC expression and endothelial ensheathing of BVI in tumor biopsies could be used to stratify patients that may benefit from an anti-angiogenic drug treatment targeting the BVI endothelial coat. In contrast to

BVI, we have found that LVI (here observed in MaCa and PDAC) do not exhibit an endothelial layer nor TNC expression thus likely not responding well to anti-angiogenic treatment.

In summary, our study has described the composition of metastatic vascular invasions in blood vessels, BVI, and has revealed that they are different from lymphatic vessel invasions, LVI. By using a murine metastasis model with abundant or no TNC expression, we have identified host-derived TNC as an important component of BVI and that TNC increases endothelial layering and tumor cell survival, cellular plasticity and extravasation, involving TGF-β signaling. This information may present novel prognostic and therapeutic opportunities. Finally, as relevant immune competent transplantation models are scarce, our novel autochthonous model of cancer progression providing the opportunity to engineer the host as well as the tumor cells, recapitulating the TME and metastatic traits of the stochastic genetic model could be relevant for future mechanistic research and metastasis targeting.

Material and methods

Human cancer tissue

Human cancer tissue (mammary carcinoma (MaCa), MaCa lung metastasis, renal cell carcinoma (RCC), hepatocellular carcinoma (HCC), pancreatic neuroendocrine tumor (PNET)) from two sites, the Medical University of Vienna/General Hospital Vienna/Medical University Wien (MUW) and the Hôpital Universitaire de Strasbourg Hautepierre (HUS) was analyzed. In the MUW cohort 30 cases of histologically proven invasive MaCa with metastasis to the lung were investigated. In the HUS cohort, 35 breast cancer specimen were collected (November 2013 – October 2014) and selected according to clinical annotation of present vascular invasions. Patients underwent surgical treatment at the MUW, Department of Obstetrics and Gynecology and at the Department of Surgery/Division of Thoracic Surgery (MUW cohort), at the HUS for the pancreatic and hepatic tumors, and the Nouvel Hôpital Civil for the renal tumors (HUS cohort). In the MUW cohort, in 12 cases enough material was available to perform all IHC stainings (**Table S3**). Serial sections of 2 µm were prepared and stained with antibodies specific for TNC, Factor VIII, CD31, CD34 and podoplanin by using an automated stainer (BenchMark Ultra, Roche/Ventana). Immunohistochemical staining was carried out in accordance with the manufacturer's instructions (Ventana Medical Systems). Immunohistochemical staining for platelets (CD61) was performed using the LEICA BOND III automated Immunostainer. In the HUS cohort, 35 patients with mammary carcinoma including 29 ductal invasive carcinomas and 5 lobular invasive carcinomas were included (**Table S4**). In addition, tumor tissue from 7 PDAC, 9 RCC, 9 HCC and 5 PNET was selected according to clinical annotations of present vascular invasions (HUS cohort) (**Table S4**). Four µm thick paraffin sections were analyzed upon staining with HE or incubation with antibodies against TNC, CD31, and podoplanin (D2-40) by using an

automated stainer (BenchMark Ultra, Roche/Ventana). Immunohistochemical staining was carried out in accordance with the manufacturer's instructions (Ventana Medical Systems). Analysis of staining results was performed by two pathologists independently (FO/RK, MUW cohort of breast cancer; AO/RK MUW cohort of RCC; GA/MPC, HUS cohort of breast cancer; GA/ZS, HUS cohort of RCC, HCC, PNET) in each center. Details can be found in **Table S2, S3 and S4** and results are summarized in **Table 1**. Ethical approval for the procedures described has been granted.

Mice

MMTV-NeuNT female mice (FVB/NCrl background) with a mutated constitutively active form of rat ErbB2 (NeuNT), expressed under control of the mouse mammary tumor virus (MMTV) regulatory region [37], were provided by Gerhard Christofori (University of Basel, Switzerland). Mice expressing NeuNT develop multifocal breast adenocarcinoma and lung metastasis; TNC +/- mice in the 129/Sv genetic background were generously donated by Reinhard Fässler [38]. Ten consecutive crosses with FVB/NCrl mice (Charles River) were done to homogenize the background. TNC +/- males were crossed with TNC +/- females to obtain TNC+/+ (WT) and TNC-/- (KO) littermates; MMTV-NeuNT mice (FVB/NCrl background) were crossed with TNC+/- mice to generate double-transgenic mice to obtain MMTV-NeuNT mice with a TNC+/+ and TNC-/- genotype. All mice were housed and handled according to the guidelines of INSERM and the ethical committee of Alsace, France (CREMEAS) (Directive 2010/63/EU on the protection of animals used for scientific purposes).

Animal experiments

Tumor size was measured every 3 or 7 days with a caliper, and tumor volume was calculated using the formula $V = (a^2 * b)/2$, where b is the longest axis and a is the

perpendicular axis to b. For the syngeneic mouse model**,** 10 x 10^6 NT193 cells were diluted in 50 µL PBS and injected orthotopically into the left fourth mammary gland. Mice were euthanized at indicated time points and mammary gland tumors and lungs were processed for histological analysis and western blot. Tissue was snap frozen in liquid nitrogen or embedded in O.C.T. (Sakura Finetek) as well as in paraffin for tissue staining.

Tissue analysis

The stereological analysis of the lung metastasis (index and number) was done as published [19]. Briefly, the left lung lobe was cut transversally into 2.0 mm thick parallel pieces, giving rise to a total of five to six pieces before paraffin embedding in parallel orientation, and cutting into 7 µm thick sections. In cases where no metastasis was found, 8 to 10 additional sections separated by 200 µm were analyzed.

HE staining

Tissue from breast tumors and lungs were prepared and fixed overnight in 4% PFA, dehydrated in 100% ethanol for 24 h, embedded in paraffin, cut in 7 µm thick sections, dewaxed and rehydrated with 100% Toluene (2 washes of 15 minutes) then incubated in 100%–70% alcohol solutions (10 minutes each) followed by a final staining with hematoxylin (Surgipath) for 5 minutes and washing with tap water or followed by IHC. Sections were further processed with differentiation solution (1% HCl in absolute ethanol, for 7 seconds), followed by washing under tap water for 10 minutes. Sections were then incubated in eosin (Harris) for 10 seconds, rinsed and dehydrated in 70% - 100% alcohol baths with rapid dips in each bath before a final wash in toluene for 15 minutes and embedded in Eukitt solution (Sigma).

Giemsa staining

Tissue was cut in 7 µm thick sections, dewaxed and stained with Giemsa (320310-0125, RAL) for 2 hours at 37°C, further processed in a 0.5% aqueous acetic acid solution, dehydrated and embedded with Eukitt solution.

Immunohistochemistry

Paraffin embedded tissue was rehydrated and the antigens were unmasked by boiling in 10 mM pH 6 citrate solution for 20 minutes. Cooled slides were washed and incubated in a peroxide solution (0.6% H2O2, 0.1% triton X-100 in PBS) to eliminate endogenous peroxidase activity. Non-specific binding sites were blocked with a blocking solution (5% normal goat serum in PBS) for one hour at room temperature (RT) and then avidin/biotin receptors were blocked by using the avidin/biotin blocking kit as recommended by the manufacturer (Vector). Slides were incubated with the first antibody overnight at 4°C in a humidified container. Next day, slides were washed and incubated for 45 minutes at room temperature with a secondary antibody (coupled to biotin). The detection of peroxidase was done using the Elite ABC system (VECTASTAIN) with DAB (Vector) as substrate. Finally, tissue was stained with hematoxylin, dehydrated and embedded in Eukitt solution. Proliferation and apoptosis were quantified as events per area upon staining for Ki-67 and cleaved caspase-3, respectively.

Immunofluorescence staining

Tissue was air-dried and unspecific signals were reduced with blocking solution (5% normal goat or donkey serum in PBS) for one hour at RT. Tissue sections were incubated with the primary antibody overnight at 4°C in a humidified container. The following day the primary antibody was removed and tissue was incubated with a fluorescent secondary

antibody for one hour at RT. Slides were washed and incubated with DAPI (Sigma) to visualize the nuclei (10 minutes at RT). Excess of dye was removed and tissue was embedded with FluorSaveTM Reagent (Calbiochem). Fluorescent signal was analyzed with a Zeiss Axio Imager Z2 microscope. The staining procedure (fixation, blocking, antibody dilution) and image acquisition setting (microscope, magnification, light intensity, exposure time) were kept constant per experiment and genetic conditions. Quantification of immunofluorescent microscopic images was done by the ImageJ (National Institutes of Health) software using a constant threshold. The expression of TNC was scored according to the signal extent and intensity of the mosaic picture of the whole tumor. A typical fibrillar TNC staining with the MTn12 antibody in the stroma around the tumor cells was considered as positive signal (no signal was seen with the secondary antibody alone). The extent of TNC staining was scored by the percentage of the positively stained area. The stained area in each region of interest was scored as 0 for staining less than 5 %, as 1 for 5–25 %, 2 for 25–50 %, 3 for 50–75 %, and 4 for more than 75 % of the stained area. The intensity of staining was scored as 0, 1, 2 and 3 representing no staining, mild (weak but detectable above control), moderate (distinct) and intense (strong) staining, respectively. The percentage of positively stained area and intensity of staining were multiplied to produce a weighted score [61].

qPCR analysis

Total RNA was prepared using TriReagent (Life Technologies) according to the manufacturer's instructions. RNA was reverse transribed (MultiScribe reverse transcriptase, Applied Biosystems) and qPCR was done on cDNA (diluted 1:5 in water) using a 7500 Real Time PCR machine (Applied Biosystems) with a SYBR green reaction mixture or Taqman reaction mixture (Applied Biosystems). Data were normalized by using a Taqman mouse *Gapdh* Endogenous Control (4333764T, Life Technology) and fold

induction was calculated using the comparative Ct method (-ddCt). Primers used for qPCR are listed in **Table S1.**

Immunoblotting

Cell lysates were prepared in lysis buffer (25 mM Tris-HCl pH 7.6, 150 mM NaCl,1% NP-40, 1% sodium deoxycholate, 0.1% SDS) supplemented with protease inhibitor (Roche) and Phosphatase Inhibitor Cocktail (Santa Cruz). Protein concentration was determined with a Bradford Assay (BioRad). After addition of Laemmli buffer (Biorad), 20-30 µg protein lysate was separated by SDS-PAGE in precasted 4-20 % gradient gels (Biorad), transferred onto nitrocellulose membranes (Biorad) using TransBlot Turbo™ Transfer System (Biorad), blocked with 5 % Blocking-Grade blocker (Biorad) in 0.1% Tween 20-PBS and incubated with the primary (overnight at 4°C) and secondary antibodies (one hour at RT) in 1.5 % Blocking-Grade Blocker in 0.1 %Tween 20-PBS. Protein bands were detected with the Amersham ECL Western Blotting detection reagent (GE Healthcare) or SuperSignal™ West Femto Maximum Sensitivity Substrate (ThermoFisher).

Immunofluorescence staining of cells

Cells were fixed in 4 % PFA for 10 minutes, permeabilized in PBS-Triton 0.1 % for 10 minutes, incubated with the primary antibody overnight at 4 °C, secondary antibody for one hour at RT, DAPI, embedded with FluorSaveTM Reagent (Calbiochem) and analyzed with an Zeiss Axio Imager Z2 microscope.

Antibodies

The primary antibodies are shown in **Table S2**. Secondary antibodies were ECL horseradish peroxidase-linked (1/1000): anti-rat (NA935) and anti-rabbit (NA934V) (GE

Healthcare). Secondary goat or donkey antibodies were fluorescently labeled (1/1000): anti-mouse, anti-rabbit, anti-rat, anti-guinea pig and anti-goat IgG (Jackson Laboratory).

Cell culture

NT193 cells derived from a MMTV-NeuNT primary tumor [20] were cultured in DMEM medium with 4.5 g/L glucose (GIBCO) supplemented with 10 % of inactivated fetal bovine serum, penicillin (10 000 U/ml) and streptomycin (10 mg/ml). Cells were maintained at 37°C in a humidified atmosphere of 5 % CO_2.

Treatment with TGF-β and GW788388

Cells were starved in the absence of serum overnight before treatment with human recombinant TGF-β1 (100-21, PEPROTECH), recombinant TNC (purified as described [62]) or the TGF-β type I receptor inhibitor GW 788388 (Selleckchem). Cells were pretreated with the inhibitor for 45 minutes prior to incubation with TNC, TGF-β and platelets, respectively. All reagents were diluted following the manufacturer's instructions.

Transduction of cells

Silencing of *Tnc* in mouse cells was done by short hairpin (sh) mediated gene expression knock down (KD). Lentiviral particles with shRNA vectors (Sigma-Aldrich) specific for *Tnc* were used. sh1, TRCN0000312137, sequence 5'-CCGGCCCG GAACTGAATATGGGATTCTCGAGAATCCCATATTCAGTTCCGGGTTTTTG-3'; sh2, TRCN0000312138, 5'-CCGGGCATCAACACAACCAGTCTAACTCGAGTTAGACTGG TTGTGTTGATGCTTTTTG-3'. Lentiviral particles encoding a non-targeting shRNA vector were used as a control (SHC202V, Sigma-Aldrich). Transduced cells were selected with

normal medium supplemented with 10 µg/ml puromycin (ThermoFisher) and the selection pressure was maintained in all in vitro experiments.

Spheroid assay

NT193 cells were seeded at 5000 cells per 100 µL together with TNC (10 µg/ml) or PBS-Tween-20 (0.01%) in 96 well plates with round bottom pre-coated with 10 µg/ml of poly-HEMA (Sigma) for 24 hours to allow spheroid formation and then were embedded in OCT for further immunostaining analysis.

Wound healing assay

NT193 cells (2×10^5) were grown to confluency in 24-well plates for 24 hours. Confluent cell monolayers were treated two hours with mitomycin-C (Sigma) at 2 µg/ml to inhibit proliferation before application of a scratch wound with a pipet tip. Cell debris was removed by PBS washing before addition of serum-free medium supplemented with the indicated molecules. Images of the wounding area were acquired immediately after scratching and then in the same field after 24 hours. The relative wound closure was quantified by measuring the surface of the cell-free area at the time of injury and at the end point of the experiment.

Cell death assessment with caspase 3/7 activity assay

Caspase 3/7 activity assay (Promega) was performed according to the manufacturer's instructions. Briefly, 2000 cells/well were plated overnight in 96-well plates. Cells were treated as described for the indicated time period and then cell apoptosis was induced by staurosporine (1 µg/ml, Sigma) for 24 hours. To measure caspase 3/7 activity, 75 µL of caspase Glo 3/7 reagent was added to each well for one hour with constant shaking at

RT. Luminescence was measured using a TriStar² LB942 multidetection microplate reader.

Preparation of washed platelets

Blood was drawn from the abdominal aorta of adult FVB/NCrl mice anesthetized intraperitoneally with a mixture of xylazine (20 mg/kg, Rompun, Bayer) and ketamine (100 mg/kg, Imalgene 1000, Merial). Platelets were washed using ACD-anticoagulated whole blood as previously described [63].

Enzyme-linked immunosorbent assay (ELISA)

Subconfluent NT193 sh2TNC cells ($5x10^5$) were grown on plastic (6 wells plates) for 24 hours in full medium (10%FCS), serum starved (no serum) overnight, and incubated for 24 hours in serum-free DMEM containing 0.01% Tween-20 (CTRL), TGF-β (10 ng/ml), TNC (10 μg/ml, 35 nM (MW 280kDa)), TNC-FBG (10 μg/ml, 383 nM (MW 26.1kDa)) and TNC-FnIII3-5 (10 μg/ml, 327 nM (MW 30.6kDa), respectively. All proteins were synthetized and purified as described [64]. Cells were separated from the conditioned medium by centrifugation and, secreted TGF-β was determined using ELISA (RnD Systems DY1679) following the manufacturer`s recommendations.

Statistical analysis

The GraphPad Prism software (version 6) was used for graphical representations of data and statistical analyses to assess significance of observed differences. All parametric (unpaired Student t test with Welch's correction in case of unequal variance) and non-parametric tests (Mann-Whitney) were performed in a two-tailed fashion. To compare the proportion of BVI and parenchymal metastases, Fisher's exact test or Chi-square test was

used. Mean ± SEM. p values < 0.05 were considered as statistically significant (*p < 0.05; **p < 0.01; ***p < 0.001; ****p < 0.0001).

References

[1] J.E. Talmadge, I.J. Fidler, AACR Centennial Series: The Biology of Cancer Metastasis: Historical Perspective, Cancer Research. 70 (2010) 5649–5669. doi:10.1158/0008-5472.CAN-10-1040.

[2] S. Gkountela, F. Castro-Giner, B.M. Szczerba, M. Vetter, J. Landin, R. Scherrer, I. Krol, M.C. Scheidmann, C. Beisel, C.U. Stirnimann, C. Kurzeder, V. Heinzelmann-Schwarz, C. Rochlitz, W.P. Weber, N. Aceto, Circulating Tumor Cell Clustering Shapes DNA Methylation to Enable Metastasis Seeding, Cell. 176 (2019) 98-112.e14. doi:10.1016/j.cell.2018.11.046.

[3] K. Lapis, S. Paku, L.A. Liotta, Endothelialization of embolized tumor cells during metastasis formation, Clin. Exp. Metastasis. 6 (1988) 73–89.

[4] E.A. Rakha, S. Martin, A.H.S. Lee, D. Morgan, P.D.P. Pharoah, Z. Hodi, D. MacMillan, I.O. Ellis, The prognostic significance of lymphovascular invasion in invasive breast carcinoma, Cancer. 118 (2012) 3670–3680. doi:10.1002/cncr.26711.

[5] T. Fujii, R. Yajima, T. Hirakata, T. Miyamoto, T. Fujisawa, S. Tsutsumi, Y. Ynagita, M. Iijima, H. Kuwano, Impact of the Prognostic Value of Vascular Invasion, but Not Lymphatic Invasion, of the Primary Tumor in Patients with Breast Cancer, Anticancer Res. 34 (2014) 1255–1259.

[6] I. Soerjomataram, M.W.J. Louwman, J.G. Ribot, J.A. Roukema, J.W.W. Coebergh, An overview of prognostic factors for long-term survivors of breast cancer, Breast Cancer Research and Treatment. 107 (2008) 309–330. doi:10.1007/s10549-007-9556-1.

[7] M.J. Bissell, W.C. Hines, Why don't we get more cancer? A proposed role of the microenvironment in restraining cancer progression, Nature Medicine. 17 (2011) 320–329. doi:10.1038/nm.2328.

[8] A.J. Minn, G.P. Gupta, P.M. Siegel, P.D. Bos, W. Shu, D.D. Giri, A. Viale, A.B. Olshen, W.L. Gerald, J. Massagué, Genes that mediate breast cancer metastasis to lung, Nature. 436 (2005) 518–524. doi:10.1038/nature03799.

[9] T. Oskarsson, S. Acharyya, X.H.-F. Zhang, S. Vanharanta, S.F. Tavazoie, P.G. Morris, R.J. Downey, K. Manova-Todorova, E. Brogi, J. Massagué, Breast cancer cells produce tenascin C as a metastatic niche component to colonize the lungs, Nature Medicine. 17 (2011) 867–874. doi:10.1038/nm.2379.

[10] K.S. Midwood, M. Chiquet, R.P. Tucker, G. Orend, Tenascin-C at a glance, J Cell Sci. 129 (2016) 4321–4327. doi:10.1242/jcs.190546.

[11] F. Saupe, A. Schwenzer, Y. Jia, I. Gasser, C. Spenlé, B. Langlois, M. Kammerer, O. Lefebvre, R. Hlushchuk, T. Rupp, M. Marko, M. van der Heyden, G. Cremel, C. Arnold, A. Klein, P. Simon-Assmann, V. Djonov, A. Neuville-Méchine, I. Esposito, J. Slotta-Huspenina, K.-P. Janssen, O. de Wever, G. Christofori, T. Hussenet, G. Orend, Tenascin-C Downregulates Wnt Inhibitor Dickkopf-1, Promoting

Tumorigenesis in a Neuroendocrine Tumor Model, Cell Reports. 5 (2013) 482–492. doi:10.1016/j.celrep.2013.09.014.

[12] J. Insua-Rodríguez, M. Pein, T. Hongu, J. Meier, A. Descot, C.M. Lowy, E. De Braekeleer, H.-P. Sinn, S. Spaich, M. Sütterlin, A. Schneeweiss, T. Oskarsson, Stress signaling in breast cancer cells induces matrix components that promote chemoresistant metastasis, EMBO Mol Med. 10 (2018). doi:10.15252/emmm.201809003.

[13] J.F. Talts, G. Wirl, M. Dictor, W.J. Muller, R. Fässler, Tenascin-C modulates tumor stroma and monocyte/macrophage recruitment but not tumor growth or metastasis in a mouse strain with spontaneous mammary cancer, J. Cell. Sci. 112 (Pt 12) (1999) 1855–1864.

[14] S.F. Tavazoie, C. Alarcón, T. Oskarsson, D. Padua, Q. Wang, P.D. Bos, W.L. Gerald, J. Massagué, Endogenous human microRNAs that suppress breast cancer metastasis, Nature. 451 (2008) 147–152. doi:10.1038/nature06487.

[15] L. Bouchard, L. Lamarre, P.J. Tremblay, P. Jolicoeur, Stochastic appearance of mammary tumors in transgenic mice carrying the MMTV/c-neu oncogene, Cell. 57 (1989) 931–936.

[16] W.J. Muller, E. Sinn, P.K. Pattengale, R. Wallace, P. Leder, Single-step induction of mammary adenocarcinoma in transgenic mice bearing the activated c-neu oncogene, Cell. 54 (1988) 105–115.

[17] P.M. Siegel, W. Shu, R.D. Cardiff, W.J. Muller, J. Massagué, Transforming growth factor β signaling impairs Neu-induced mammary tumorigenesis while promoting pulmonary metastasis, Proceedings of the National Academy of Sciences. 100 (2003) 8430–8435. doi:10.1073/pnas.0932636100.

[18] C. Spenlé, I. Gasser, F. Saupe, K.-P. Janssen, C. Arnold, A. Klein, M. van der Heyden, J. Mutterer, A. Neuville-Méchine, M.-P. Chenard, D. Guenot, I. Esposito, J. Slotta-Huspenina, N. Ambartsumian, P. Simon-Assmann, G. Orend, Spatial organization of the tenascin-C microenvironment in experimental and human cancer, Cell Adh Migr. 9 (2015) 4–13. doi:10.1080/19336918.2015.1005452.

[19] B.S. Nielsen, L.R. Lund, I.J. Christensen, M. Johnsen, P.A. Usher, L. Wulf-Andersen, T.L. Frandsen, K. Danø, H.J.G. Gundersen, A Precise and Efficient Stereological Method for Determining Murine Lung Metastasis Volumes, The American Journal of Pathology. 158 (2001) 1997–2003. doi:10.1016/S0002-9440(10)64671-8.

[20] A. Arpel, P. Sawma, C. Spenlé, J. Fritz, L. Meyer, N. Garnier, I. Velázquez-Quesada, T. Hussenet, S. Aci-Sèche, N. Baumlin, M. Genest, D. Brasse, P. Hubert, G. Crémel, G. Orend, P. Laquerrière, D. Bagnard, Transmembrane Domain Targeting Peptide Antagonizing ErbB2/Neu Inhibits Breast Tumor Growth and Metastasis, Cell Reports. 8 (2014) 1714–1721. doi:10.1016/j.celrep.2014.07.044.

[21] J.T. O'Connell, H. Sugimoto, V.G. Cooke, B.A. MacDonald, A.I. Mehta, V.S. LeBleu, R. Dewar, R.M. Rocha, R.R. Brentani, M.B. Resnick, E.G. Neilson, M. Zeisberg, R. Kalluri, VEGF-A and Tenascin-C produced by S100A4+ stromal cells are important for metastatic colonization, Proceedings of the National Academy of Sciences. 108 (2011) 16002–16007. doi:10.1073/pnas.1109493108.

[22] A. Dongre, R.A. Weinberg, New insights into the mechanisms of epithelial–mesenchymal transition and implications for cancer, Nature Reviews Molecular Cell Biology. 20 (2019) 69. doi:10.1038/s41580-018-0080-4.

[23] C.K.S. Meikle, C.A. Kelly, P. Garg, L.M. Wuescher, R.A. Ali, R.G. Worth, Cancer and Thrombosis: The Platelet Perspective, Frontiers in Cell and Developmental Biology. 4 (2017). doi:10.3389/fcell.2016.00147.

[24] P.H. Mangin, N. Receveur, V. Wurtz, T. David, C. Gachet, F. Lanza, Identification of five novel 14-3-3 isoforms interacting with the GPIb-IX complex in platelets, Journal of Thrombosis and Haemostasis. 7 (2009) 1550–1555. doi:10.1111/j.1538-7836.2009.03530.x.

[25] M. Labelle, S. Begum, R.O. Hynes, Direct Signaling between Platelets and Cancer Cells Induces an Epithelial-Mesenchymal-Like Transition and Promotes Metastasis, Cancer Cell. 20 (2011) 576–590. doi:10.1016/j.ccr.2011.09.009.

[26] T. Rupp, B. Langlois, M.M. Koczorowska, A. Radwanska, Z. Sun, T. Hussenet, O. Lefebvre, D. Murdamoothoo, C. Arnold, A. Klein, M.L. Biniossek, V. Hyenne, E. Naudin, I. Velazquez-Quesada, O. Schilling, E. Van Obberghen-Schilling, G. Orend, Tenascin-C Orchestrates Glioblastoma Angiogenesis by Modulation of Pro- and Anti-angiogenic Signaling, Cell Reports. 17 (2016) 2607–2619. doi:10.1016/j.celrep.2016.11.012.

[27] A. Radwanska, D. Grall, S. Schaub, S.B. la F. Divonne, D. Ciais, S. Rekima, T. Rupp, A. Sudaka, G. Orend, E. Van Obberghen-Schilling, Counterbalancing anti-adhesive effects of Tenascin-C through fibronectin expression in endothelial cells, Scientific Reports. 7 (2017). doi:10.1038/s41598-017-13008-9.

[28] K.J. Cheung, V. Padmanaban, V. Silvestri, K. Schipper, J.D. Cohen, A.N. Fairchild, M.A. Gorin, J.E. Verdone, K.J. Pienta, J.S. Bader, A.J. Ewald, Polyclonal breast cancer metastases arise from collective dissemination of keratin 14-expressing tumor cell clusters, Proceedings of the National Academy of Sciences. 113 (2016) E854–E863. doi:10.1073/pnas.1508541113.

[29] Y. Zhang, R.A. Weinberg, Epithelial-to-mesenchymal transition in cancer: complexity and opportunities, Front. Med. 12 (2018) 361–373. doi:10.1007/s11684-018-0656-6.

[30] K. Nagaharu, X. Zhang, T. Yoshida, D. Katoh, N. Hanamura, Y. Kozuka, T. Ogawa, T. Shiraishi, K. Imanaka-Yoshida, Tenascin C Induces Epithelial-Mesenchymal Transition–Like Change Accompanied by SRC Activation and Focal Adhesion Kinase Phosphorylation in Human Breast Cancer Cells, The American Journal of Pathology. 178 (2011) 754–763. doi:10.1016/j.ajpath.2010.10.015.

[31] J. Xu, S. Lamouille, R. Derynck, TGF-β-induced epithelial to mesenchymal transition, Cell Research. 19 (2009) 156–172. doi:10.1038/cr.2009.5.

[32] A. Singh, J. Settleman, EMT, cancer stem cells and drug resistance: an emerging axis of evil in the war on cancer, Oncogene. 29 (2010) 4741–4751. doi:10.1038/onc.2010.215.

[33] L. De Laporte, J.J. Rice, F. Tortelli, J.A. Hubbell, Tenascin C Promiscuously Binds Growth Factors via Its Fifth Fibronectin Type III-Like Domain, PLoS ONE. 8 (2013) e62076. doi:10.1371/journal.pone.0062076.

[34] C. Kolliopoulos, C.-Y. Lin, C.-H. Heldin, A. Moustakas, P. Heldin, Has2 natural antisense RNA and Hmga2 promote Has2 expression during TGFβ-induced EMT in breast cancer, Matrix Biol. (2018). doi:10.1016/j.matbio.2018.09.002.

[35] L.A. Griggs, N.T. Hassan, R.S. Malik, B.P. Griffin, B.A. Martinez, L.W. Elmore, C.A. Lemmon, Fibronectin fibrils regulate TGF-β1-induced Epithelial-Mesenchymal Transition, Matrix Biology. 60–61 (2017) 157–175. doi:10.1016/j.matbio.2017.01.001.

[36] A. Pezzolo, F. Parodi, D. Marimpietri, L. Raffaghello, C. Cocco, A. Pistorio, M. Mosconi, C. Gambini, M. Cilli, S. Deaglio, F. Malavasi, V. Pistoia, Oct-4+/Tenascin C+ neuroblastoma cells serve as progenitors of tumor-derived endothelial cells, Cell Research. 21 (2011) 1470–1486. doi:10.1038/cr.2011.38.

[37] T. Sugino, T. Yamaguchi, G. Ogura, A. Saito, T. Hashimoto, N. Hoshi, S. Yoshida, S. Goodison, T. Suzuki, Morphological evidence for an invasion-independent metastasis pathway exists in multiple human cancers, BMC Medicine. 2 (2004). doi:10.1186/1741-7015-2-9.

[38] R.V. Iozzo, M.A. Gubbiotti, Extracellular matrix: The driving force of mammalian diseases, Matrix Biology. 71–72 (2018) 1–9. doi:10.1016/j.matbio.2018.03.023.

[39] N.K. Karamanos, A.D. Theocharis, T. Neill, R.V. Iozzo, Matrix modeling and remodeling: A biological interplay regulating tissue homeostasis and diseases, Matrix Biology. 75–76 (2019) 1–11. doi:10.1016/j.matbio.2018.08.007.

[40] N. Dandachi, C. Hauser-Kronberger, E. Moré, B. Wiesener, G.W. Hacker, O. Dietze, G. Wirl, Co-expression of tenascin-C and vimentin in human breast cancer cells indicates phenotypic transdifferentiation during tumour progression: correlation with histopathological parameters, hormone receptors, and oncoproteins, The Journal of Pathology. 193 (2001) 181–189. doi:10.1002/1096-9896(2000)9999:9999<::AID-PATH752>3.0.CO;2-V.

[41] X. Shen, R.H. Kramer, Adhesion-mediated squamous cell carcinoma survival through ligand-independent activation of epidermal growth factor receptor, Am. J. Pathol. 165 (2004) 1315–1329. doi:10.1016/S0002-9440(10)63390-1.

[42] Y. Katsuno, D.S. Meyer, Z. Zhang, K.M. Shokat, R.J. Akhurst, K. Miyazono, R. Derynck, Chronic TGF-β exposure drives stabilized EMT, tumor stemness, and

cancer drug resistance with vulnerability to bitopic mTOR inhibition, Sci. Signal. 12 (2019) eaau8544. doi:10.1126/scisignal.aau8544.

[43] T. Sugino, T. Kusakabe, N. Hoshi, T. Yamaguchi, T. Kawaguchi, S. Goodison, M. Sekimata, Y. Homma, T. Suzuki, An Invasion-Independent Pathway of Blood-Borne Metastasis, Am J Pathol. 160 (2002) 1973–1980.

[44] V.L.T. Ballard, A. Sharma, I. Duignan, J.M. Holm, A. Chin, R. Choi, K.A. Hajjar, S.-C. Wong, J.M. Edelberg, Vascular tenascin-C regulates cardiac endothelial phenotype and neovascularization, The FASEB Journal. 20 (2006) 717–719. doi:10.1096/fj.05-5131fje.

[45] N. Aceto, A. Bardia, D.T. Miyamoto, M.C. Donaldson, B.S. Wittner, J.A. Spencer, M. Yu, A. Pely, A. Engstrom, H. Zhu, B.W. Brannigan, R. Kapur, S.L. Stott, T. Shioda, S. Ramaswamy, D.T. Ting, C.P. Lin, M. Toner, D.A. Haber, S. Maheswaran, Circulating Tumor Cell Clusters Are Oligoclonal Precursors of Breast Cancer Metastasis, Cell. 158 (2014) 1110–1122. doi:10.1016/j.cell.2014.07.013.

[46] D.G. Duda, A.M.M.J. Duyverman, M. Kohno, M. Snuderl, E.J.A. Steller, D. Fukumura, R.K. Jain, Malignant cells facilitate lung metastasis by bringing their own soil, Proc. Natl. Acad. Sci. U.S.A. 107 (2010) 21677–21682. doi:10.1073/pnas.1016234107.

[47] R.G. Oshima, J. Lesperance, V. Munoz, L. Hebbard, B. Ranscht, N. Sharan, W.J. Muller, C.A. Hauser, R.D. Cardiff, Angiogenic acceleration of Neu induced mammary tumor progression and metastasis, Cancer Res. 64 (2004) 169–179.

[48] B. Langlois, F. Saupe, T. Rupp, C. Arnold, M. van der Heyden, G. Orend, T. Hussenet, AngioMatrix, a signature of the tumor angiogenic switch-specific matrisome, correlates with poor prognosis for glioma and colorectal cancer patients, Oncotarget. 5 (2014) 10529–10545.

[49] R. Lauria, F. Perrone, C. Carlomagno, M. De Laurentiis, A. Morabito, C. Gallo, E. Varriale, G. Pettinato, L. Panico, G. Petrella, The prognostic value of lymphatic and blood vessel invasion in operable breast cancer, Cancer. 76 (1995) 1772–1778.

[50] N. Knijn, U.E.M. van Exsel, M.E. de Noo, I.D. Nagtegaal, The value of intramural vascular invasion in colorectal cancer - a systematic review and meta-analysis, Histopathology. 72 (2018) 721–728. doi:10.1111/his.13404.

[51] S. Okada, S. Mizuguchi, N. Izumi, H. Komatsu, M. Toda, K. Hara, T. Okuno, T. Shibata, H. Wanibuchi, N. Nishiyama, Prognostic value of the frequency of vascular invasion in stage I non-small cell lung cancer, Gen Thorac Cardiovasc Surg. 65 (2017) 32–39. doi:10.1007/s11748-016-0720-6.

[52] M.R.S. Siddiqui, C. Simillis, C. Hunter, M. Chand, J. Bhoday, A. Garant, T. Vuong, G. Artho, S. Rasheed, P. Tekkis, A.-M. Abulafi, G. Brown, A meta-analysis comparing the risk of metastases in patients with rectal cancer and MRI-detected extramural vascular invasion (mrEMVI) vs mrEMVI-negative cases, Br. J. Cancer. 116 (2017) 1513–1519. doi:10.1038/bjc.2017.99.

[53] T.A. Klingen, Y. Chen, I.M. Stefansson, G. Knutsvik, K. Collett, A.L. Abrahamsen, H. Aase, H. Aas, T. Aas, E. Wik, L.A. Akslen, Tumour cell invasion into blood vessels is significantly related to breast cancer subtypes and decreased survival, J. Clin. Pathol. 70 (2017) 313–319. doi:10.1136/jclinpath-2016-203861.

[54] V.F. Marinho, K. Metze, F.S. Sanches, G.F. Rocha, H. Gobbi, Lymph vascular invasion in invasive mammary carcinomas identified by the endothelial lymphatic marker D2-40 is associated with other indicators of poor prognosis, BMC Cancer. 8 (2008) 64. doi:10.1186/1471-2407-8-64.

[55] G.G. Van den Eynden, I. Van der Auwera, S.J. Van Laere, C.G. Colpaert, P. van Dam, L.Y. Dirix, P.B. Vermeulen, E.A. Van Marck, Distinguishing blood and lymph vessel invasion in breast cancer: a prospective immunohistochemical study, Br J Cancer. 94 (2006) 1643–1649. doi:10.1038/sj.bjc.6603152.

[56] K.E. Roberts, D. Hamele-Bena, A. Saqi, C.A. Stein, R.P. Cole, Pulmonary tumor embolism: a review of the literature, Am. J. Med. 115 (2003) 228–232.

[57] N.S. Vasudev, A.R. Reynolds, Anti-angiogenic therapy for cancer: current progress, unresolved questions and future directions, Angiogenesis. 17 (2014) 471–494. doi:10.1007/s10456-014-9420-y.

[58] V. Zambonin, A. De Toma, L. Carbognin, R. Nortilli, E. Fiorio, V. Parolin, S. Pilotto, F. Cuppone, F. Pellini, D. Lombardi, G.P. Pollini, G. Tortora, E. Bria, Clinical results of randomized trials and “real-world” data exploring the impact of Bevacizumab for breast cancer: opportunities for clinical practice and perspectives for research, Expert Opin Biol Ther. 17 (2017) 497–506. doi:10.1080/14712598.2017.1289171.

[59] K.C. Aalders, K. Tryfonidis, E. Senkus, F. Cardoso, Anti-angiogenic treatment in breast cancer: Facts, successes, failures and future perspectives, Cancer Treat. Rev. 53 (2017) 98–110. doi:10.1016/j.ctrv.2016.12.009.

[60] M. Rajabi, S. Mousa, The Role of Angiogenesis in Cancer Treatment, Biomedicines. 5 (2017) 34. doi:10.3390/biomedicines5020034.

[61] M. Shi, X. He, W. Wei, J. Wang, T. Zhang, X. Shen, Tenascin-C induces resistance to apoptosis in pancreatic cancer cell through activation of ERK/NF-κB pathway, Apoptosis. 20 (2015) 843–857. doi:10.1007/s10495-015-1106-4.

[62] W. Huang, R. Chiquet-Ehrismann, J.V. Moyano, A. Garcia-Pardo, G. Orend, Interference of tenascin-C with syndecan-4 binding to fibronectin blocks cell adhesion and stimulates tumor cell proliferation, Cancer Res. 61 (2001) 8586–8594.

[63] J.-P. Cazenave, P. Ohlmann, D. Cassel, A. Eckly, B. Hechler, C. Gachet, Preparation of Washed Platelet Suspensions From Human and Rodent Blood, in: Platelets and Megakaryocytes, Humana Press, New Jersey, 2004: pp. 013–028. doi:10.1385/1-59259-782-3:013.

[64] K. Midwood, S. Sacre, A.M. Piccinini, J. Inglis, A. Trebaul, E. Chan, S. Drexler, N. Sofat, M. Kashiwagi, G. Orend, F. Brennan, B. Foxwell, Tenascin-C is an endogenous activator of Toll-like receptor 4 that is essential for maintaining

inflammation in arthritic joint disease, Nat. Med. 15 (2009) 774–780. doi:10.1038/nm.1987.

Acknowledgement

We are grateful for technical support by Christiane Arnold, Fanny Steinbach, Anna Brown and the personnel of the animal facility. This work was supported by grants from Worldwide Cancer Research/AICR (14-1070), INCa (TENPLAMET), Ligue Régional contre le Cancer CCIR Est, INSERM and University Strasbourg to GO, INCa (TENPLAMET) to PM, National Natural Science Foundation of China (Grant No. 81802655) to ZS and fellowship grants from the Chinese Scholarship Council (ZS) and the Mexican scholarship program Conacyt (IVQ). KSM is supported by Arthritis Research UK.

Autor contribution

ZS, IVQ and TH developed the genetic and orthotopic grafting model. ZS, IVQ, DM, AY, TH, CA, CD, WE and CS performed experiments, analyzed and interpreted the data. OL, AK, AB, MvdH and CB provided technical assistance. GA, FO, AO, MPC, CM and RK provided, analyzed and interpreted data from human cancer patients. PM supervised the platelet study. GC provided the MMTV-NeuNT mice. GC, TL, CAF and KM critically reviewed the manuscript and interpreted data. ZS, IVQ and GO conceptualized and wrote the manuscript. Grants to GO financed this study.

Competing financial interests

The authors declare no competing financial interests.

Supplemental information for Sun et al., **Tenascin-C increases lung metastasis by impacting blood vessel invasions**

Supplemental Table S1 Summary of vascular invasion characteristics in human cancers

Supplemental Table S2 Patient information

Supplemental Table S3 List of primer sequences used for qPCR

Supplemental Table S4 List of antibodies

Table 1 Summary of vascular invasion characteristics in human carcinomas

Number of tissues with vascular invasions	Number of tissues with BVI or LVI	Number of tissues with endothelialized vascular invasions	Number of tissues with TNC layer	Number of tissues with floating or attached vascular invasions
HCC (HUS) (9)	BVI (9/9), LVI (0/9)	BVI (9/9)	BVI (9/9)	attached (7/9) floating (2/9)
RCC (HUS) (9)	BVI (9/9), LVI (0/9)	BVI (9/9)	BVI (9/9)	attached (9/9)
PNET (HUS) (5)	BVI (5/5), LVI (0/5)	BVI (5/5)	BVI (5/5)	attached (5/5)
PDAC (HUS) (7)	BVI (0/7), LVI (7/7)	LVI (0/7)	LVI (0/7)	floating (7/7)
Ductal invasive MaCa (HUS) (29)	BVI (0/29), LVI (29/29)	LVI (0/29)	LVI (0/25)	floating (29/29)
Lobular invasive MaCa (HUS) (5)	BVI (0/5), LVI (5/5)	LVI (0/5)	LVI (0/5)	floating (5/5)
MaCa (MUW) (1)	BVI (0/12), LVI (1/12)	LVI (0/1)	LVI (0/1)	floating (1/1)
MaCa lung metastasis (MUW) (5)	BVI (0/12), LVI (5/12)	LVI (0/5)	LVI (0/5)	floating (5/5)

Summary of immunohistochemical analysis of human carcinoma tissue and detection of BVI or LVI in hepatocellular carcinoma (HCC), renal cell carcinoma (RCC), pancreatic neuroendocrine tumors (PNET), pancreatic ductal adenocarcinoma (PDAC), invasive mammary carcinoma (MaCa) and MaCa lung metastasis of the HUS and MUW cohorts of patients. Expression of TNC and presence of endothelial cells (flat nuclei in HE images, CD31 staining) in BVI is depicted. Note that BVI / LVI are either separated from the vessel wall and appear as embolus-like (floating) structures or are connected to the vessel wall protruding into the vessel lumen (attached). Note further two groups of vascular invasions, BVI with invasions mostly into veins of highly vascularized tumors (HCC, RCC, PNET) which are ensheathed by an endothelial monolayer and express TNC at the rim, similar to what has been seen in BVI of the MMTV-NeuNT model. In the second group of tissues derived from PDAC, MaCa and MaCa lung metastasis, we only noticed LVI. These LVI did not express TNC nor were surrounded by endothelial cells. Whether BVI and LVI exist in the same tumor has to be addressed in the future.

Table S2 Patient information

Number	G	Age (D)	Diagnosis	Grading, staging	Age (M)
1	F	60	MaCa IDC NST	G1, pT1c, pN0	65
2	F	43	Multifocal MaCa IDC NST	G1 and G2, pT2, pN1b-iii	49
3	F	49	MaCa IDC NST	G3, pT?, pN3b	50
4	F	68	Multifocal MaCa IDC NST	G2, pT2, pN1b-iii	78
5	F	64	MaCa ILC	G2, pT1c, pN0	70
6	F	57	Medullary carcinoma	pT2	67
7	F	38	MaCa IDC NST	G3, pT2, pN0	42
8	F	63	MaCa IDC NST	G3, pT1c	64
9	F	62	MaCa IDC NST	G2, pT2, pN1a, L1	63
10	F	53	MaCa IDC NST	G3, pT2, pN0	67
11	F	47	MaCa IDC NST	G2, pT2	54
12	F	58	MaCa IDC NST	G3, ypT1c, ypN1a, L0	60
13	F	81	MaCa IDC NST	pT2N1	
14	F	66	MaCa ILC	pT2N1	
15	F	74	MaCa ILC	pT2N1mi	
16	F	58	MaCa IDC NST	ypT2N1	
17	F	63	MaCa ILC	pT3N0	
18	F	70	MaCa IDC NST	ypT1aN0	
19	F	63	MaCa IDC NST	pT1cN0	
20	F	79	MaCa IDC NST	pT2N2	
21	F	59	MaCa IDC NST	pT2N0	
22	F	61	MaCa ILC	pT2N1	
23	F	70	MaCa IDC NST	pT4bN3a	
24	F	45	MaCa IDC NST	pT2N1	
25	F	47	MaCa IDC NST	pT2N1	
26	F	58	MaCa IDC NST	pT2cN1	
27	F	43	MaCa IDC NST	pT2N1	
28	F	52	MaCa IDC NST	pT4bN1a	
29	F	68	MaCa IDC NST	pT2N1	
30	F	64	MaCa IDC NST	pT1cN1a	
31	F	76	MaCa IDC NST	pT1cN0	
32	F	63	MaCa IDC NST	pT1cN0	
33	F	70	MaCa IDC NST	pT1cN1	
34	F	45	MaCa IDC NST	ypT2N0	
35	F	60	MaCa IDC NST	pT2N0	
36	F	34	MaCa IDC NST	pT2N1	
37	F	82	MaCa IDC NST	pT4aNx	
38	F	50	MaCa IDC NST	pT2N0	
39	F	50	MaCa ILC	pT3N1	
40	F	43	MaCa IDC NST	ypT1cN0	
50	F	79	MaCa IDC NST	pT2N1	
51	F	31	MaCa IDC NST	pT2N0	
52	F	51	MaCa IDC NST	pT1bN0	
53	F	83	MaCa IDC NST	pT1cN2a	
54	F	40	MaCa IDC NST	pT2N2a	
55	F	71	RCC	pT3aNxL1V1R0	
56	M	57	RCC	pT1bNxL0V1R0	
57	M	74	RCC	pT3aNxl	

58	F	19	RCC	pT3aN1L1V1R0	
59	M	53	RCC	pT4N1L1V1R2	
60	F	82	RCC	pT3aNXL0V0R0	
61	M	75	RCC	pT1aNXL0V1R0	
62	M	77	RCC	pT3aNxL0V0R0	
63	M	56	RCC sarcomatoid	pT3aNXL0V1R0	
64	M	58	HCC	pT4V1	
65	M	63	HCC	pT3bN0V1	
66	M	61	HCC	pT3bN0V1	
67	M	59	HCC	pT4N0V1	
68	M	75	HCC	pT4V1	
69	M	57	HCC	pT4N0V1	
70	M	58	HCC	pT4NXV1	
71	M	72	HCC	pT2N0M1	
72	M	58	HCC	pT4NXV1	
73	M	61	PNET G2	pT1cV1Pn1N0R0	
74	M	76	PNET G1	pT3V2Pn1R0N0	
75	M	63	PNET G2	pT3N0L0V1Pn1R0	
76	M	45	PNET G2	ypT3N1LXV1Pn1R1	
77	M	56	PNET G1	pT1N0V1L0Pn0R0	
78	M	77	PDAC	pT3N1R0	
79	M	62	PDAC	pT3N1R1M1	
80	F	67	PDAC	pT3N1R0	
81	M	66	PDAC	pT3N1M1R0	
82	M	60	PDAC (BC)	pT4N1M1R1	
83	F	79	PDAC	pT3N1L1V1Pn1R1*	
84	F	76	APBA	pT4N1R0	

Human cancer tissue from mammary carcinoma (MaCa) and associated lung metastasis of mammary carcinoma patients and, renal cell carcinoma (RCC), hepatocellular carcinoma (HCC), pancreatic neuroendocrine tumor (PNET) and pancreatic adenocarcinoma (PDAC) with annotation of tumor vascular invasions was analyzed as described in the methods section. Gender (F, female, M, male), age at diagnosis, grading (G1, G2, G3), staging (TNM classification, https://www.uicc.org/resources/tnm) with pathological lymph node involvement (pN) and distant metastatic spread (M) is shown. APBA, Ampullary pancreato-biliary adenocarcinoma. PDAC (BC), biliary adenocarcinoma. For MaCa: Age at diagnosis (D), age at lung metastasectomy (M), IDC NST, invasive ductal carcinoma, no special type (according to WHO classification), ILC, invasive lobular carcinoma; ypT, tumor stage after chemotherapy; mi, micrometastasis.

Table S3 Primer sequences used for qPCR

GENE	Forward primer	Reverse primer
E-cadherin	CAGCCTTCTTTTCGGAAGACT	GGTAGACAGCTCCCTATGACTG
vimentin	CCAACCTTTTCTTCCCTGAAC	TTGAGTGGGTGTCAACCAGA
slug	CTCACCTCGGGAGCATACAG	GACTTACACGCCCCAAGGATG
twist	AGTGTTTGGCAGGGGACA	CCCATCCCCTGGGTATCT
zeb1	GCCAGCAGTCATGATGAAAA	TATCACAATACGGGCAGGTG
fibonectin	GATGCCGATCAGAAGTTTGG	GGTTGTGCAGATCTCCTCGT
tenascin-C	CAGGGATAGACTGCTCTGAGG	CATTGTCCCATGCCAGATTT
MMP9	ACGACATAGACGGCATCCA	GCTGTGGTTCAGTTGTGGTG
PAI-1	GGCACCTTTGAATACTCAGGA	TTTCCCAGAGACCAGAACCA
Axin2	CTGCTGGTCAGGCAGGAG	TGCCAGTTTCTTTGGCTCTT
snail	Tapman probe, Hs00195591_m1, ThermoFisher	

Table S4 Antibodies

Antigen	Host	Antibody name	Source	Dilution	Application
Akt	rabbit	4691	Cell Signaling	1/1000	WB
α-SMA	mouse	A2547	Sigma-Aldrich	1/400	IF
CD31	rat	550274	BD pharmigen	1/200	IF
CD31	mouse	JC/70A/M823	DAKO	1/20	IHC
CD31	rabbit	clone EP78/ AC-0083	Epitomics	manual	IHC (HUS)
CD34	mouse	Q-Bond 10	Novocastra	1/50	IHC (AKH)
CD41	rat	11024	Abcam	2µg/ml	IF
CD45	rat	550566	BD pharmigen	1/500	IF
CD61/platelet glycoprotein IIIa	mouse	Clone 2f2/ 161M-15	Cell Marque	Ready to use	IHC (AKH)
Cleaved caspase-3	rabbit	9661	Cell Signaling	1/600	IHC
Cytokeratin CK8/18	guinea pig	GP11	PROGEN	1/500	IF
D2-40/ podoplanin	mouse	322M-18	Cell Marque	Ready to use	IHC (AKH)
D2-40/ podoplanin	mouse	M3619	BenchMark Ultra, Roche/Ventana	manual	IHC (HUS)
E-cadherin	rat	13-1900	Life Technology	1/200 IF 1/1000 WB	IF, WB
ErbB2	rabbit	MA5-13675	ThermoFisher	1/50	IF
Erk1/2	rabbit	9102	Cell Signaling	1/1000	WB
Factor VIII	rabbit	A082	DAKO	1/2000	IHC (AKH)
Fibronectin	rabbit	F3648	Sigma-Aldrich	1/200	IF
FSP1	rabbit	Mts1/S100a4	Ambartsumian (1996)	1/200	IF
GPIbβ	rat	RAM.1	Mangin (2009)	3µg/ml	IF
Ki-67	rabbit	RM-9106	ThermoFisher	1/600	IHC
P-Akt	rabbit	4060	Cell Signaling	1/1000	WB
P-Erk1/2	mouse	9106	Cell Signaling	1/1000	WB
p-Smad2	rabbit	3108	Cell Signaling	1/1000	WB
Pan-laminin	rabbit	Ln6 7S	Simo et al.	1/2000	IF
Smad2/3	rebbit	3102	Cell Signaling	1/1000	WB
TGF-β	rabbit	3711	Cell Signaling	1/1000	WB
TNC	rat	MTn12	Aufderheide (1988)	2µg/ml IF 0.4µg/ml WB	IF, WB
TNC	mouse	NCL-TENAS-C	Novocastra	1/50	IHC (AKH)
TNC	mouse	BC24	Sigma	1/4000	IHC
Vimentin	rabbit	2707-1	EPITOMICS	1/500 IF 1/1000 WB	IF, WB

IF, immunofluorescence staining, IHC, immunohistochemical staining, WB, western blot. Ambartsumian et al., 1996, Oncogene 13, 1621 - 30, Aufderheide et al., 1988, J Cell Biol 100, 2341-9, Mangin et al., 2009, J. Thromb. Haemost **7**, 1550–55.